CNWRA 98-008

EFFECTS OF ENVIRONMENTAL FACTORS ON CONTAINER LIFE

Prepared for

Nuclear Regulatory Commission
Contract NRC-02-97-009

Prepared by

Center for Nuclear Waste Regulatory Analyses
San Antonio, Texas

July 1998

EFFECTS OF ENVIRONMENTAL FACTORS ON CONTAINER LIFE

Prepared for

Nuclear Regulatory Commission
Contract NRC-02-97-009

Prepared by

S. Brossia
D. Dunn
N. Sridhar

Center for Nuclear Waste Regulatory Analyses
San Antonio, Texas

PREVIOUS REPORTS IN SERIES

Number	Name	Date Issued
CNWRA 91-004	A Review of Localized Corrosion of High-Level Nuclear Waste Container Materials—I	April 1991
CNWRA 91-008	Hydrogen Embrittlement of Candidate Container Materials	June 1991
CNWRA 92-021	A Review of Stress Corrosion Cracking of High-Level Nuclear Waste Container Materials—I	August 1992
CNWRA 93-003	Long-Term Stability of High-Level Nuclear Waste Container Materials: I—Thermal Stability of Alloy 825	February 1993
CNWRA 93-004	Experimental Investigations of Localized Corrosion of High-Level Nuclear Waste Container Materials	February 1993
CNWRA 93-014	A Review of the Potential for Microbially Influenced Corrosion of High-Level Nuclear Waste Containers	June 1993
CNWRA 94-010	A Review of Degradation Modes of Alternate Container Designs and Materials	April 1994
CNWRA 94-028	Environmental Effects on Stress Corrosion Cracking of Type 316L Stainless Steel and Alloy 825 as High-Level Nuclear Waste Container Materials	October 1994
CNWRA 95-010	Experimental Investigations of Failure Processes of High-Level Radioactive Waste Container Materials	May 1995
CNWRA 96-004	Thermal Stability and Mechanical Properties of High-Level Radioactive Waste Container Materials: Assessment of Carbon and Low-Alloy Steels	May 1996
CNWRA 97-010	An Analysis of Galvanic Coupling Effects on the Performance of High-Level Nuclear Waste Container Materials	August 1997
CNWRA 98-004	Effect of Galvanic Coupling Between Overpack Materials of High-Level Nuclear Waste Containers—Experimental and Modeling Results	March 1998

ABSTRACT

Localized corrosion of Ni-base Alloys 825, 625, and C-22 as well as that of A516 steel was investigated in a range of simulated near-field repository environments. A relationship between the repassivation potential for pitting and crevice corrosion and the chemical composition of the near-field environment was obtained for each of the materials using a variety of test methods. Crevice corrosion tests performed with A516 steel specimens identified conditions where severe preferential attack can occur. Long-term tests performed with the Ni-base alloys suggest the near-field environment may be sufficiently aggressive to initiate localized corrosion of Alloys 825 and 625 in the absence of highly efficient galvanic coupling to the A516 steel outer overpack. Alloy C-22, however, was found to be extremely corrosion resistant and not prone to localized attack in the simulated near-field environments.

CONTENTS

CONTENTS (cont'd)

FIGURES

FIGURES (cont'd)

TABLES

ACKNOWLEDGMENTS

This report was prepared to document work performed by the Center for Nuclear Waste Regulatory Analyses (CNWRA) for the Nuclear Regulatory Commission (NRC) under Contract No. NRC-02-97-009. The activities reported here were performed on behalf of the NRC Office of Nuclear Material Safety and Safeguards, Division of Waste Management. The report is an independent product of the CNWRA and does not necessarily reflect the views or regulatory position of the NRC.

The authors gratefully acknowledge useful discussions with G. Cragnolino, as well as his technical review, the programmatic review of B. Sagar, and the editorial review of B. Long. Appreciation is due to J. Gonzalez for assistance in preparation of this report. The authors also acknowledge the laboratory work performed by K. Gruss, W. Machowski, and S. Clay.

QUALITY OF DATA: Sources of data are referenced in each chapter. CNWRA-generated laboratory data contained in this report meet quality assurance (QA) requirements described in the CNWRA QA Manual. Data from other sources, however, are freely used. The respective sources of non-CNWRA data should be consulted for determining levels of QA.

ANALYSES AND CODES: SigmaPlot (Version 4.0.1) and Grapher (Version 1.23) computer codes were used for analyses contained in this report. These are commercial computer codes and are not controlled under the CNWRA Technical Operating Procedure–18 (Development and Control of Scientific and Engineering Software).

EXECUTIVE SUMMARY

The U.S. Department of Energy (DOE) strategy for radioactive waste containment and isolation for the proposed repository at the Yucca Mountain (YM) is to target near-complete containment of radionuclides within the waste packages (WPs) for thousands of years and limit the dose to any member of the public throughout the compliance period. The proposed repository is located in an arid site with a low annual precipitation rate and a low flow of groundwater into the repository horizon to minimize degradation of the containers by corrosion. A double metallic barrier concept has been incorporated into the WP design in an attempt to prolong the time during which the radioactive waste can be contained. In the current design, a thick corrosion allowance material (carbon steel is the primary candidate) is intended to provide a gamma radiation shield while corrosion occurs at a slow and predictable rate. After the outer barrier is perforated by corrosion, the corrosion resistant inner barrier (Ni-base alloy) will continue to contain the radionuclides. Three key assumptions made by the DOE in the calculations of WP performance are (i) corrosion of A516 carbon steel in humid air or aqueous environments will be essentially uniform with any localized corrosion having a depth to width aspect ratio of 1.5, (ii) localized corrosion of A516 steel in the form of pitting may occur under alkaline aqueous conditions, and (iii) galvanic coupling of the inner corrosion resistant barrier to the outer corrosion allowance barrier will delay pitting corrosion of the inner barrier, extending the lifetime of the WP to many thousands of years.

In support of the Nuclear Regulatory Commission High-Level Nuclear Waste Program, the Center for Nuclear Waste Regulatory Analyses is developing a performance assessment capability for the purpose of evaluating the overall performance of the proposed repository at YM. As part of the activities conducted initially in the Container Life and Source Term and later in the Total-System Performance Assessment and Integration Key Technical Issues, the Engineered Barrier System Performance Assessment Code (EBSPAC) Version 1.1 was developed as a deterministic code to provide a means for evaluating the WP lifetime and radionuclide release rates. The WP lifetimes are calculated by determining the type and rate of corrosive attack. For the outer steel barrier, corrosion is assumed to occur when the relative humidity of the repository is greater than the critical relative humidity necessary for the condensation of a thin water film on the WP surface. Localized corrosion of the WP barrier materials is assumed to be initiated only when the calculated corrosion potential of the barrier exceeds the repassivation potential for localized attack in an alkaline HCO_3^-/CO_3^{2-} environment. At corrosion potentials below the repassivation potential, degradation of the inner barrier occurs at a slow rate governed by the passive current density. Pitting corrosion is assumed to occur without an induction time when the corrosion potential exceeds the repassivation potential. The main objective of laboratory investigations of container performance reported here is to provide input into EBSPAC to improve the ability of the code to estimate both the onset of corrosion and the corrosion penetration rates.

Laboratory investigations were conducted to (i) determine the effects of chloride concentration, temperature, and pH on the repassivation potential of A516 steel; (ii) identify possible conditions where deep pits could propagate through the outer barrier, and (iii) examine the mechanism responsible for repassivation of localized corrosion. The repassivation potential was found to be dependent on chloride concentration over the range spanning from 2×10^{-4} to 4 M. Increasing the pH from 9.5 to 11.0 did not have a significant impact on the repassivation potential. Evaluation of the severity of localized corrosion damage to A516 steel specimens held at potentials above the repassivation potential as a function of environmental conditions was also performed. No systematic relationship was found between the severity of pitting attack and either solution temperature or carbonate to chloride concentration ratios. For crevice corrosion, the severity of attack increased as the temperature increased and as the carbonate to chloride concentration ratio decreased.

Investigation of the conditions inside pits during propagation and repassivation revealed that a ferrous chloride salt film forming at high metal dissolution rates stabilized the pit propagation rate. Repassivation of pitting corrosion, however, did not occur when the salt film dissolved.

A regression equation for the repassivation of crevice corrosion on Alloy 625, obtained as a function of chloride concentration, revealed that the performance of this material is better than Alloy 825 at chloride concentrations below 0.1 M. For more concentrated chloride solutions, the difference in the repassivation potentials for these materials was found to be insignificant. In contrast, the repassivation potential of Alloy C-22 was much greater than those of Alloys 825 or 625. Long-term corrosion tests performed with Alloy 825 specimens suggest this material will suffer localized attack in an air-saturated, 1,000 ppm (0.028 M) chloride solution at 95 °C. Alloy 625 may also suffer from localized attack under similar conditions. Crevice corrosion of C-22 was only observed in a 4 M chloride solution at 95 °C when the potential of the specimen was greater than 825 mV_{SHE}. The high repassivation potential of Alloy C-22 suggest that WPs constructed of this material would be virtually immune from pitting or crevice corrosion in solutions containing less than 4 M chloride. Galvanic corrosion tests identified conditions where the efficiency of galvanic coupling prevented the localized corrosion of Alloy 825. Inefficient galvanic coupling that may allow the onset of localized corrosion occurred when the candidate WP materials were separated by a variety of corrosion products.

Future work necessary to enhance the capabilities of WP performance assessment modeling was identified. The formation of deep localized corrosion penetrations into A516 steel needs to be fully addressed to predict the performance of the outer barrier. The possible detrimental effects of fabrication methods used to construct the outer barrier may also have a significant impact on WP performance. Preferential corrosion in the welded regions and the segregation of impurities as a result of welding processes may compromise the integrity of the A516 steel barrier.

Several outstanding issues were also identified for the candidate Ni-base inner barrier materials. Stress corrosion cracking susceptibility of Alloy C-22 has been reported under conditions where this material should be resistant to localized corrosion. Fabrication methods used to construct the inner WP barrier may also have a significant influence on the performance of the Ni-base materials. Evolution of the container designs to include new materials such as titanium alloys may require consideration of additional failure mechanisms such as hydrogen embrittlement. Finally, the performance of the WP materials under heat transfer and alternate wet and dry conditions postulated to occur as a result of fracture flow and dripping of condensed water enriched with salts on the WP must be evaluated.

1 INTRODUCTION

1.1 BACKGROUND

The U.S. Department of Energy (DOE) safety strategy for the proposed high-level waste (HLW) repository at Yucca Mountain (YM) (U.S. Department of Energy, 1998) relies on four key attributes of an unsaturated repository system: (i) limited water contacting the waste packages (WPs), (ii) long WP lifetime, (iii) slow rate of release of radionuclides from the waste form, and (iv) concentration reduction during transport through engineered and natural barriers. Containers are key components of the WP and are relied on to provide long WP lifetime. Long container lifetimes benefit the overall system performance in many ways: (i) the radiation source term is reduced due to decay, (ii) the spent fuel is protected from contact with air during the initial high temperature period thus reducing its susceptibility to oxidation and spalling, and (iii) the uncertainties in the performance of the geologic medium during the high temperature period are reduced. The placement of the proposed repository horizon in the unsaturated zone combined with the decay heat from the HLW may provide an extended period of low relative humidity during which the container materials can be expected to accomplish their function adequately. The uncertainty in the chemical composition of the water that may eventually contact the containers is large. Evaporation and refluxing of vadose zone water, combined with percolating meteoric water, may result in a wide concentration range of anionic species such as chloride, sulfate, carbonate, and bicarbonate. Therefore, understanding the long-term performance of the container materials under a wide range of anticipated near-field environmental conditions is necessary.

The Nuclear Regulatory Commission (NRC) refocused its prelicensing program (Sagar, 1996) by identifying 10 key technical issues (KTIs). It intends provide timely feedback to the DOE on potentially significant site, design, or assessment vulnerabilities through issue resolution status reports (IRSR) and develop and exercise independent performance assessments. Container Life and Source Term (CLST) is one of the 10 KTIs aimed at evaluating the adequacy of the engineered barrier subsystem in the context of their contribution to the overall system performance. The CLST IRSR (Nuclear Regulatory Commission, 1998) identified corrosion as an important subissue and described the current status of resolution of this subissue at the staff level.

The DOE WP design continues to evolve, but for the viability assessment (VA) the design of an A516 carbon steel outer overpack and a Ni-base alloy (Alloy C-22) inner overpack is being considered (TRW Environmental Safety Systems, Inc., 1997). The principal attribute of carbon steel is its expected behavior as a typical corrosion allowance material undergoing relatively predictable, uniform corrosion. Under some environmental conditions, however, carbon steel may form a protective surface film and, depending on the presence of aggressive anions such as Cl^-, may exhibit localized corrosion. The principal attribute of a corrosion resistant material, such as Alloy C-22, is its low corrosion rate owing to an adherent and protective passive film. Under some environmental conditions, however, corrosion resistant materials may undergo rapid penetration by localized corrosion. Hence an important topic identified in the CLST IRSR is the delineation of the environmental conditions in which carbon steel and Ni-base alloys, such as 825, 625, and C-22, may be penetrated by deep pits. The purpose of this report is to provide input to the IRSRs for developing resolution of these issues. An additional goal is to improve the container corrosion models in the NRC/Center for Nuclear Waste Regulatory Analyses (CNWRA) Total-System Performance Assessment code (TPA) (Mohanty and McCartin, 1998) through updated parameters and conceptual models.

1.2 PREVIOUS LITERATURE

1.2.1 Carbon Steels

The factors influencing the performance of carbon steel in the repository environment have been reviewed previously (Sridhar et al., 1994; Vinson et al., 1995; Cragnolino et al., 1998). Carbon steels, in principle, are binary alloys of iron and carbon with other alloying elements present, either added intentionally to produce specific desired properties or inadvertently introduced that can be detrimental to material properties. The other elements that are sometimes present in carbon steel include chromium, niobium, molybdenum, nickel, manganese, silicon, sulfur and phosphorous. Under many conditions, carbon steels exhibit uniform, general corrosion. As such, it is a relatively simple matter to predict the life expectancy of engineered structures composed of carbon steel. Under some circumstances, however, carbon steel can undergo localized corrosion, either in the form of pitting or crevice corrosion. Because localized corrosion rates are generally considerably more rapid than general corrosion and localized corrosion can occur in regions not easily accessible for visual examination (e.g., at the contact point between the WP and the pier), this form of attack is particularly insidious. As a result, considerable effort has been devoted to examining the conditions under which localized corrosion of carbon steels can occur as well as determining propagation rates of localized corrosion.

Even though a number of investigations have been conducted on the localized corrosion of carbon steel, the principal uncertainty is the possibility of pit penetration through a 10-cm thick carbon steel container without considerable lateral broadening of the pit. The maximum depth of pits observed in field studies of buried steel specimens is on the order of 0.5 mm over a 16-yr exposure period (Vinson et al., 1995). On the other hand, considerable information is available on localized corrosion depths of steel pipelines, some of them as part of public record. The measurements of pit depths on pipelines (Vieth and Kiefner, 1994) indicate that pits as deep as 9.5 mm have been observed over a time period spanning years to decades. Typically, the pits appear as multiple penetrations spanning a significant length on the order of several centimeters.

The corrosion of meteorites and archeological iron objects over a much longer time period (centuries to hundreds of thousands of years) has been reviewed (Johnson and Francis, 1980; Buchwald and Clarke, 1989; Turgoose, 1985). Buchwald and Clarke (1989) observed that antarctic meteorites showed deep penetration of corrosion even in a relatively arid climate. They attributed the deep penetration to the melting of ice due to the absorption of solar radiation by the dark meteorites and formation of small amounts of liquid water, the presence of small chloride concentrations in the antarctic ice (on the order of a few ppm), the generation of high chloride concentrations at the metal-solution interface (up to 6 percent) due to electromigration of chloride, and the formation of the mineral akaganeite (β-FeOOH), which can occlude large concentrations of chloride in its lattice structure. Buchwald and Clarke (1989) concluded that continued localized corrosion penetration is possible under these circumstances, albeit slowly as a result of low temperatures, because of the continued presence of chloride at the head of the corrosion front. They also concluded that the continued corrosion of meteoritic iron is not from the presence of $FeCl_2$ (Lawrencite), but akaganeite. Turgoose (1985; 1989) analyzed the deterioration of unearthed iron objects from soil and marine environments and suggested that the rapid deterioration of the unearthed iron objects is because of the combination of large concentrations of chloride in the form of ferrous chloride complexes in pits and the cathodic reduction of oxygen outside the pits. The objects did not corrode rapidly under buried conditions because of the anaerobic conditions. Turgoose did not invoke the necessity of akaganeite for the deterioration of these objects, but suggested that akaganeite forms as a result of oxidation of iron chloride already present

in the pits. He also suggested that the low relative humidities (approximately 18 percent) needed for the onset of corrosion in the presence of ferrous chloride is a result of the hydration equilibrium between $FeCl_2 \cdot 4H_2O$ and $FeCl_2 \cdot 2H_2O$.

It is clear from the literature that, despite many decades of study, the environmental factors and mechanisms that stabilize localized corrosion of steel have been only incompletely understood. Specific areas that need to be addressed to resolve the subissue related to the corrosion of carbon steel are

- The combination of pH, anionic concentrations, and temperatures that may lead to localized corrosion of steel rather than uniform corrosion
- The factors that govern deep pit propagation such that penetration of the 10-cm thick steel overpack may occur

1.2.2 Ni-Base Alloys

Unlike iron and steel, the database on long-term performance of these alloys is relatively small. A brief history of the C-type alloys is given in this section to provide the reader an understanding of the origin and applications of these alloys. The history of development of these alloys has been described in greater detail elsewhere (Tawancy et al., 1983; Manning and Schöbel, 1986). The Ni-base alloys for use in corrosive applications arose to prominence in the 1920s. The early alloys, such as Hastelloy Alloy C, contained high carbon (about 0.1 wt %) and high silicon (about 0.5 wt %) and hence were metallurgically quite unstable. Because of their instability toward carbide precipitation, they were essentially casting alloys. In the 1940s, a lower carbon (about 0.05 wt %) Alloy C was made using oxygen blowing, which enabled production of wrought forms. In the 1960s, it was realized that silicon increases the tendency of these alloys to precipitate M_6C type carbides (where M is a combination of Cr and Mo) that were deleterious to weld corrosion resistance. Taking advantage of this knowledge to improve alloy properties became possible with the advent of argon oxygen decarburization (AOD) process in the 1960s, which enabled lowering the carbon content (Klein et al., 1981). The large-scale development of the electroslag remelting (ESR) process in the 1960s enabled production of low sulfur containing alloys. These improvements in processing resulted in the development of Alloy C-276 with less than 0.01 percent carbon in 1967. Alloy 625 was developed originally for aerospace applications and contained relatively high carbon (about 0.03 percent) to provide high temperature strength. To prevent grain boundary carbide precipitation, about 3.5 percent niobium (columbium) was added. The increased knowledge of phase transformation in these alloys and its relationship to the electronic structure of the alloys resulted in the development of Alloy C-4 in 1976, which possessed improved metallurgical stability, but at the expense of some loss in corrosion resistance. Alloy C-4 was considered in the German HLW program and was a candidate alloy in the U.S. repository and Waste Isolation Pilot Plant (WIPP) programs.

Alloys C-276 and C-4, with their relatively low chromium (about 15.5 wt %), were not as corrosion resistant in some oxidizing environments as Alloy 625, which has 21.5 percent Cr. Alloy 625, however, with a lower Mo and W content, did not have as high a resistance to localized corrosion as the C-type alloys. Development of Alloy C-22 in 1979 resulted from an optimization of these three compositions. Large-scale production of Alloy C-22 began in 1981. It was initially used in the chemical process industry, but eventually in a variety of other industrial applications, such as flue gas desulfurization, pulp and paper bleaching, and off-shore oil and gas production. Other modifications of Alloy C-22, such as Alloys 59, 686, and 2000, have been produced in the 1980s and 1990s.

The methodology for long-term prediction of the localized corrosion of Alloy 825 has been described in detail in a previous report (Dunn et al., 1997). Several field test results were cited in this report and the consistency of the field test results with the repassivation potential concept was indicated. There is a paucity of repassivation potential data for Alloys C-276, C-22, and 625 since these alloys are highly resistant to localized corrosion over a wide range of chloride concentrations at temperatures up to the boiling point under ambient pressures. The most common localized corrosion parameter reported for these alloys is the critical pitting/crevice temperature. This parameter is measured by immersing noncreviced or creviced specimens in highly acidic, oxidizing chloride solutions (i.e., $FeCl_3$) for time periods varying from 24 to 240 hr at various temperatures and visually examining the specimens for evidence of localized corrosion after the test. The temperature at which localized corrosion is observed or below which localized corrosion is not observed (the difference between these depending on the temperature intervals) is considered to be the critical temperature. Unfortunately, because the critical temperature is a function of potential, chloride concentration, and test duration, it is difficult to use these measurements to determine service life.

Renner et al. (1986) performed crevice corrosion tests on Alloy C-22 in 6 wt % $FeCl_3$ (1.1 M chloride). The measured redox potential in this environment (using platinum) ranged from 925 mV_{SHE} at 18 °C to 955 mV_{SHE} at 90 °C. The pH of this solution was about 1.3. They found that the critical crevice corrosion temperature (CCT) was greater than 80 °C (the highest temperature tested). Hibner (1986) measured the CCT of Alloy C-22 in the same solution but used a slightly different procedure and found the critical crevice temperature to be 54 °C. In contrast to Renner et al. (1986), who used the same specimen at different temperatures without any surface polishing between temperatures, Hibner (1986) polished the specimens between temperature increments thereby providing fresh surface for the corrodent. Manning et al. (1983) measured the CCT of Alloys 625 and C-22 in a 7 vol % H_2SO_4 + 3 vol % HCl + 1 wt % $FeCl_3$ + 1 wt % $CuCl_2$ solution (total chloride of 1.7 M) to be 25 °C for Alloy 625 and 101 °C for Alloy C-22. The redox potential of this solution was about 920 mV_{SHE}. They used independent specimens at each temperature. The significant discrepancy in the measured CCT suggests that the test techniques need to be better understood. Furthermore, since corrosion potentials were not measured, it is difficult to correlate them to long-term field experience.

A review of the various laboratory and field test results of the C-type alloys and Alloy 625 suggests that the methodology for long-term prediction of localized corrosion needs to be improved and that significant uncertainty exists regarding the CCT of the alloys.

1.3 TECHNICAL APPROACH

For carbon steels, relatively short-term tests (ranging from a few hours to 168 days) were conducted to determine the environmental conditions leading to localized corrosion. It is recognized that the pH, total carbonate and chloride concentrations, and temperature influence the localized corrosion susceptibility most and hence attention was focused on these factors. High pH and carbonate concentration leads to the formation of a protective passive film. High chloride concentration leads to destabilization of protective passive films and uniform corrosion. Hence the effect of ratio of the chloride to carbonate concentration on the localized corrosion is examined. Cyclic polarization tests provide a rapid method to screen the environmental conditions but are unreliable for long-term prediction, especially for carbon steel. Hence potentiostatic tests are used to assess long-term stability of localized corrosion. The mechanisms leading to stabilization of localized corrosion, however, are difficult to determine on a large surface area because pit nucleation is a stochastic process and positioning of the measuring probe at the location where pitting would occur is extremely difficult. The stability of localized corrosion was examined using a lead-in-pencil (LIP)

type arrangement in which the location of the localized corrosion front was known (bottom of the lead-in-pencil type electrode) and the probe (in this case Raman spectrometer probe head) was focused on this front. The effect of external cathodic processes, as well as corrosion of the pit walls, can not be studied by this technique.

In the case of Ni-base alloys, investigations over the past 8 years have shown the usefulness of the repassivation potential for predicting the long-term performance of Alloy 825. It has also been shown that rapid electrochemical tests can be used to measure this parameter, provided the alloy suffers localized corrosion. Therefore, the study reported here examines the usefulness of this technique for the more corrosion resistant alloys.

The effectiveness of galvanic coupling steel to Alloy 825 to protect Alloy 825 against the occurrence of localized corrosion was examined in previous reports (Dunn and Cragnolino, 1997; 1998). The results presented in this report complete these activities.

2 EXPERIMENTAL METHODS

2.1 SPECIMENS

The chemical compositions of Alloys 825, 625, and C-22, as well as A516 steel, are shown in table 2-1. Materials were obtained in the form of mill-annealed, 12.5 mm thick plates. Geometry and dimensions of the various specimens used in this study are shown in figure 2-1. The cylindrical rod specimens (figure 2-1a) were used in cyclic potentiodynamic polarization (CPP) and potentiostatic polarization (PP) tests. They were machined to 6.3 mm (0.25 in.) in diameter and 19.06 mm (0.75 in.) to 48.6 mm (1.9 in.) in length. All of the exposed surfaces of these specimens were polished to a 600-grit finish. Figure 2-lb shows the LIP test specimens. The smaller diameter end of the specimen was enclosed by a glass tube sheath such that only the cross section was exposed to the solution. The glass tube extended beyond the end of the specimen by approximately 1 cm to form an artificial pit. The specimen was attached to a holding rod, which was bent in the shape of a "J," such that the open end of the glass sheath was facing upward. The other end of the rod remained outside the cell. Cubic specimens used in some long-term potentiostatic tests are shown in figure 2-1c. The geometry of this specimen allowed both polished and mill finished surfaces to be exposed to the solution. Specimens used for the crevice corrosion studies (both CPP and PP tests), fabricated to the dimensions shown in figure 2-ld, had 600-grit polished surfaces and an exposed surface area of approximately 20 cm^2. Square block specimens shown in figure 2-1e were used in both galvanic corrosion tests and potentiostatic pitting tests. Prior to the start of a test, all specimens were cleaned ultrasonically in detergent, rinsed in deionized (DI) water, ultrasonically cleaned in acetone, and dried. At the completion of each test, the specimens were rinsed in DI and examined. Most specimens were cleaned ultrasonically in an inhibited hydrochloric acid solution that contained 4 mL of 2-butyne-1,4-diol (35 percent aqueous solution) and 3 mL of concentrated hydrochloric acid (HCl), together with 50 mL of water or methanol to remove the corrosion products. A516 steel specimens were cleaned in methanol. A post-test visual examination was performed with an optical microscope.

2.2 TEST METHODS

2.2.1 Cyclic Polarization Tests

CPP and PP tests were used to examine the localized corrosion behavior of both Ni-based alloys and A516 carbon steel. The CPP test procedure is similar to that given in ASTM Standard G61 (American Society for Testing and Materials, 1996a), which involves scanning the potential applied to the specimen and

Table 2-1. Chemical composition (wt %) of the materials tested in this study

Material	Fe	Cr	Ni	Mo	Mn	Ti	Si	S	C	Other
Alloy 825	30.4	22.1	41.1	3.30	0.35	0.8	0.19	<0.001	0.01	1.80 Cu
Alloy 625	3.96	21.7	60.9	9.01	0.08	0.24	0.16	0.001	0.02	3.48 Nb
Alloy C-22	3.80	21.4	57.8	13.6	0.12	—	0.03	0.002	0.004	3.0 W, 0.15 V
A516 Steel	98.5	0.03	0.01	0.01	1.00	—	0.23	0.009	0.18	0.014 P

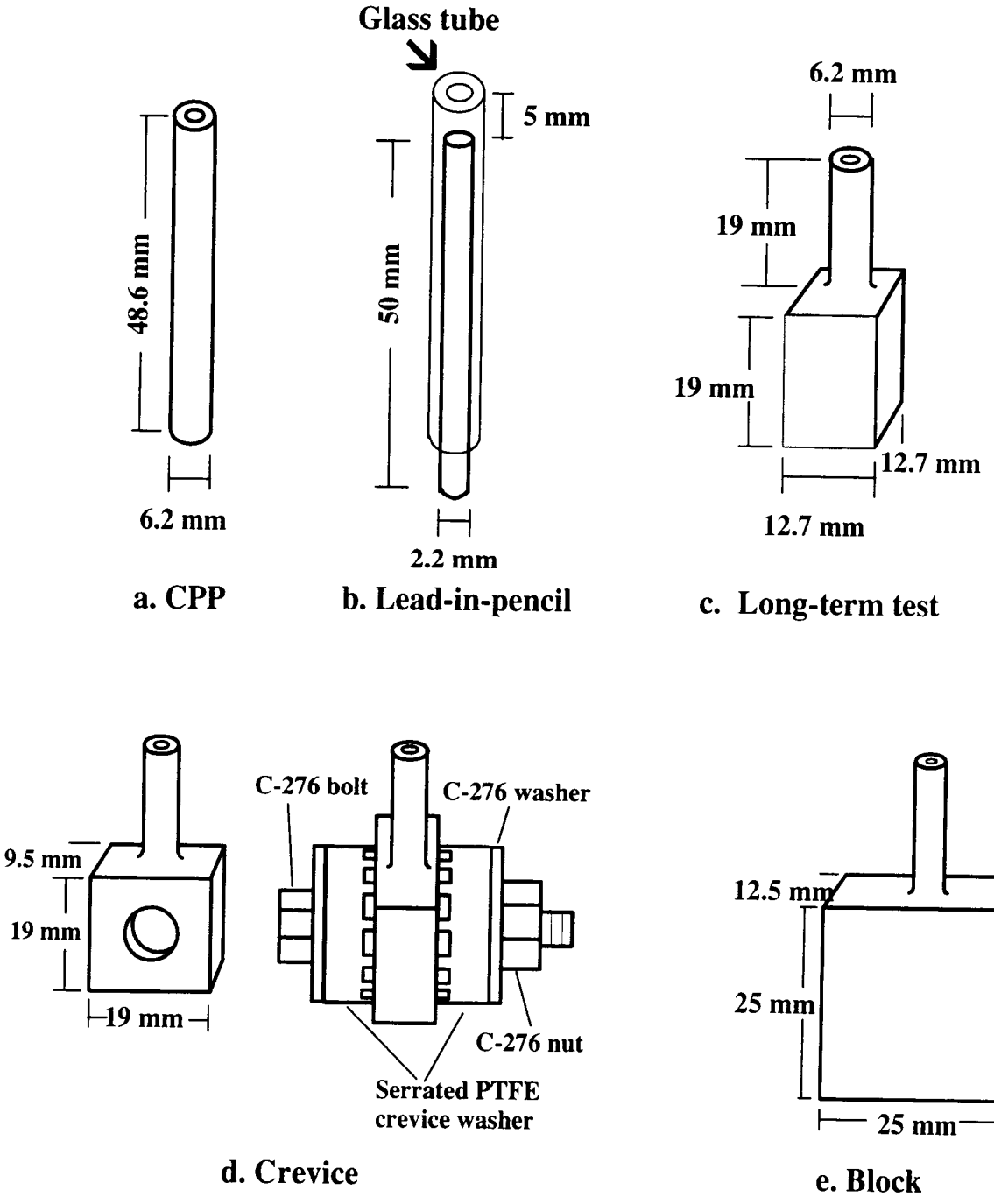

Figure 2-1. Dimensions of specimens used in this study

monitoring the current response. The PP test procedure involves stepping the potential applied to the specimen to a specified value and monitoring the current as a function of time, as discussed by Scully (1995). In both types of tests, the test apparatus consisted of a 5-port glass cell fitted with a water-cooled Allihn-type condenser and a water trap to minimize solution loss at elevated temperatures and air intrusion. Cylindrical specimens (figure 2-1a) were either fully immersed or partially immersed to avoid crevice corrosion at the electrical contact to the specimen. A salt-bridge/Luggin probe with a porous silica tip was used so the tip was in the test solution and the other end was at room temperature to minimize instability in the reference electrode from temperature fluctuations. In general, the salt-bridge was filled with test solution, except for cases where testing was performed in high resistivity media (e.g., J-13 water), in which case the salt-bridge was filled with concentrated NaCl solution to minimize noise in the system. A saturated calomel electrode (SCE) was used as a reference electrode in all experiments. All potentials reported are on the basis of the standard hydrogen scale (SHE) at ambient temperature (~22 °C) without correction for the thermal diffusion potential associated with the nonisothermal salt-bridge. A platinum (Pt) flag or graphite cylinder was used as a counter electrode. Solutions were deaerated with high purity nitrogen for 1 hr prior to introduction of the specimen and were continuously purged during testing. CPP testing was performed using EG&G Princeton Applied Research (PAR) Models VersaStat, 273, and 173/276 potentiostats controlled by a personal computer running PAR Model 352 Corrosion Software. The scans were initiated from either the open circuit potential (E_{corr}), measured at least 1 hr after immersing the specimen in solution, or at a potential cathodic to the E_{corr}. A scan rate of 0.167 mV/sec was used while the current was measured for all experiments. The scans were reversed at a current density of 5 mA/cm^2.

2.2.2 Potentiostatic Polarization Tests

PP testing was performed using an Electrosynthesis Model 440 mulitchannel potentiostat connected to a PC equipped with a Strawberry Tree ACPC-16-16, 16-bit, 16-channel, analog-digital converter (ADC) and an ACAO-12-8, 12-bit, 8-channel, digital-analog converter (DAC) running Strawberry Tree WorkbenchPC software for data acquisition and control. The sampling rate chosen was 10 Hz. The current resolution with this system is 0.125 μA. The current and potential measurements were verified independently using a Keithley Model 614 electrometer, a Keithley Model 485 picoammeter, and a Fluke 8050A Digital Multimeter. After PP testing, the specimens used in these experiments (figure 2-1d) were examined for evidence of localized corrosion (pitting/crevice) and if observed, were subjectively ranked and the accompanied weight loss determined.

2.2.3 Galvanic Corrosion Tests

Galvanic corrosion tests were performed using Alloy 825 and A516 steel cylindrical specimens (figure 2-1a). Tests were conducted in 2 L test cells with solutions containing 0.028 or 0.5 M NaCl under air-saturated or deaerated conditions. Solution pH was varied between 3 and 10.8 and temperature was 25 or 95 °C. Prior to the start of the tests a high impedance electrometer was used to measure the corrosion potentials of the specimens versus an SCE that served as the reference electrode. The specimens were then galvanically coupled through a potentiostat functioning as a zero resistance ammeter (ZRA). After galvanically coupling the specimens, the potential of the galvanic couple and the galvanic corrosion current were recorded. Tests were conducted using Alloy 825 to A516 steel area ratios in the range of 1:10 to 10:1. Each test was conducted for a period of 5 to 10 days. At the conclusion of the tests the specimens were

removed and visually inspected. The weight loss of each specimen was also measured. The galvanic potential and current density results obtained with Alloy 825 and A516 specimens were compared to predictions (Dunn and Cragnolino, 1997; Dunn et al., 1998)

Additional galvanic corrosion tests were performed to measure the potential of both A516 and Alloy 825 with a range of coupling efficiencies using specimens having square surfaces (figure 2-1e). Initial measurements were made with polished surfaces of the two materials directly coupled to each other. Coupling under inefficient conditions was simulated by using passivated, thermally oxidized, and mill scale covered specimens. The coupling efficiency was further reduced by placing a 1.5 mm thick O-ring filled with either reagent grade iron oxides, oxyhydroxides, or A516 corrosion products between the specimens.

2.2.4 Lead-in-Pencil Repassivation Tests

The E_{rp} for Alloys 625 and C-22 was measured as a function of chloride concentration using LIP specimens. Previous tests performed with Alloy 825 specimens indicated that the E_{rp} measured with LIP specimens was consistent with that measured on pitting or crevice corrosion specimens. For the LIP tests, a 1 L, reaction kettle as described in ASTM G31 (American Society for Testing and Materials, 1996b), was fitted with a fritted gas bubbler, platinum counter electrode, temperature probe, and a Luggin probe with a short salt-bridge for an SCE. A water-cooled condenser placed on top of the salt-bridge was used to maintain the solution at ambient temperature. A cotton wick, presoaked in the solution, was introduced into the salt-bridge to provide a continuous electrolyte path to the reference electrode even when air bubbles formed during the test. Tests were initiated by stepping the potential to a high value (>842 mV_{SHE}) to induce active dissolution inside the simulated pit. This value was maintained for 12–18 hr to allow the pit to grow. After pit growth had stabilized, the applied potential was decreased at a scan rate of 0.167 mV/sec. The repassivation potential was determined as the potential where the current density fell below 10^{-7} A/cm^2.

2.2.5 Long-Term Tests

The validity of using E_{rp} from short-term tests as a parameter for determining the long-term performance of container materials was tested by comparing the critical potentials obtained in CPP tests with potentiostatic tests. Potentiostatic initiation tests were conducted by polarizing both cylindrical and creviced specimens to potentials above and below the E_{rp} previously measured using the CPP technique, in a solution containing 1,000 ppm Cl^-, 85 ppm HCO_3^-, 20 ppm SO_4^{2-}, 10 ppm NO_3^-, and 2 ppm F^-, all as sodium salts. The tests were conducted in an ASTM G31 (American Society for Testing and Materials, 1996b) type reaction kettle with approximately 1,500 mL of solution maintained at 95 °C. The cell was equipped with a platinum counter electrode and a water cooled Luggin probe with a porous silica tip. An SCE, connected to the cell through a Luggin probe, was used as the reference electrode. Specimens were connected to a computer controlled multichannel potentiostat. A constant potential was applied for test intervals of 28–168 days. Between these test periods, the specimens were examined for weight loss and visible signs of corrosion while the test solution was changed. No further exposures were conducted on specimens after localized corrosion occurred.

2.2.6 Experiments on Pit Stability and Growth

In situ Raman spectroscopy was used to examine salt film precipitation in a simulated one-dimensional (1D) pit on iron. A schematic diagram of the experimental apparatus used is shown in

figure 2-2. The glass cell has four ports for the specimen, a Luggin capillary and a salt-bridge connected to an SCE reference electrode, a Pt counter electrode, and a gas bubbler with a water trap to minimize air intrusion. One side of the cell is flat to improve the accuracy of laser beam focusing. The specimen is positioned close to the flat wall of the cell to minimize the path of the laser through the bulk solution since Raman scattering from water is more intense than that from salt solutions (Sridhar and Dunn, 1997), which could lead to saturation of the charge-coupled device (CCD) detector during the acquisition times used to obtain significant signal from simulated pit solutions. All experiments were performed on 99.9985 wt % pure Fe (Johnson Matthey) in the form of a 2-mm diameter wire. The sample was polarized using an EG&G PAR Model 273 potentiostat in deaerated 0.5 M HCl + 2 M NaCl solution. The end of the electrode was covered by glass tubing that extended to form a 1D pit with an initial depth of 10 mm and an area of 0.031 cm^2. The remaining Fe wire was isolated from the solution by heat shrinkable tubing. High purity nitrogen was used to deaerate the test solution. Both the current density and the potential of the pit specimen were continuously monitored using a personal computer with a Strawberry Tree ACPC-16-16, 16-bit, 16-channel ADC running Strawberry Tree WorkbenchPC software for data acquisition with a sampling rate of 10 Hz.

Raman spectroscopy was conducted using a Kaiser Optical HoloProbe 532 dispersive system. The laser source used was a Coherent diode-pumped, solid-state, frequency-doubled Nd:YAG laser with a 532 nm wavelength. Laser light from the source is passed through 50 μm core diameter optical fibers to the probe head. Using the 50 μm incident fiber and a 62.5 μm focal length lens, the spot size is believed to be approximately 10 μm. The incident laser power used was about 10 mW. Instrument resolution was about 5 cm^{-1}. The probe head was mounted on a micrometer stage arranged to move vertically parallel to the pit

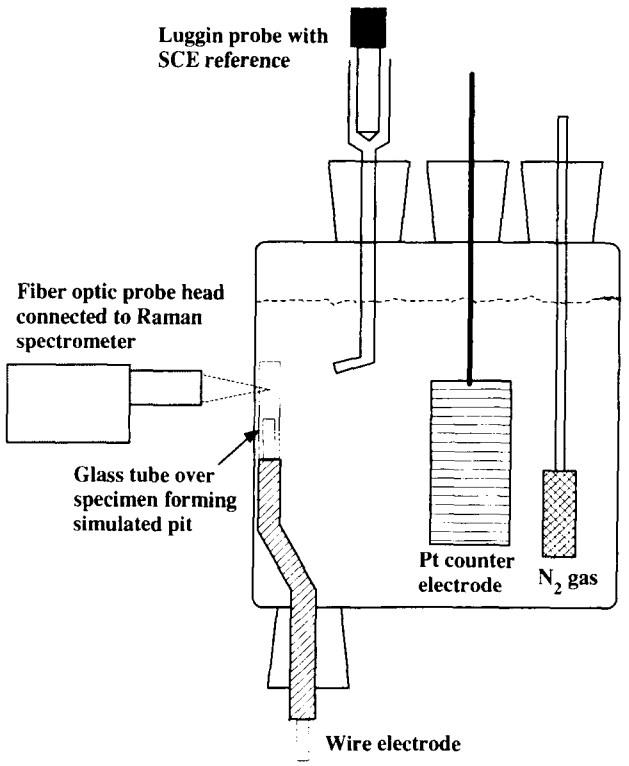

Figure 2-2. Schematic diagram of test cell used during *in situ* Raman spectroscopy examination of salt film precipitation in a simulated one-dimensional pit on iron

electrode. To facilitate examination of salt film precipitation, the probe head was mounted at a slightly oblique angle such that the laser was incident on the bottom of the pit. The spectral acquisition time used was 20 sec. Unknown compounds were identified by comparison to spectra of known reagents.

Alignment of the Raman instrument was performed at the beginning of the investigation using an argon ion source that has well defined plasma lines (Strommen and Nakamoto, 1984). Periodic verification of calibration was performed by obtaining the Raman spectra of cyclohexane and sulfur. The measured peaks associated with these compounds were within 1–2 cm^{-1} of the reported values (Strommen and Nakamoto, 1984; Degen and Newman, 1993).

3 RESULTS

3.1 LOCALIZED CORROSION OF CARBON STEEL

3.1.1 Effect of Environment on Pitting and Repassivation Potentials

The effect of chloride concentration on the pitting (E_{pit}) and repassivation (E_{rp}) potentials were determined by conducting CPP experiments as a function of chloride concentration in solutions containing a total carbonate concentration of 0.012 M as sodium carbonate (Na_2CO_3) and sodium bicarbonate ($NaHCO_3$). The HCO_3^-/CO_3^{2-} ratio was adjusted for each solution to obtain a pH of 9.5 or 11.0. CPP experiments were conducted at 25, 65, and 95 °C.

The E_{pit} and E_{rp} measured from each CPP experiment are summarized in figures 3-1 to 3-5 as a function of chloride concentration. Each curve has been fitted using linear regression and the resulting dependence of the critical potentials on chloride concentration under the conditions studied are shown in each figure. Some of these figures have also been presented elsewhere (Cragnolino et al., 1998; Mohanty et al., 1997), but all are included here for completeness. The relationships at fixed temperature and pH take the form shown in Eq. (3-1)

$$E_{crit} = E^0_{crit} - B \log[Cl^-] \tag{3-1}$$

where E^0_{crit} represents the critical potential for 1 M chloride concentration and B is the regression slope. As can be seen, E_{pit} is strongly dependent on the chloride concentration with regression slopes (B) ranging from -45 to -129 mV/pCl$^-$ (pCl$^-$=log[Cl$^-$]) at pH 9.5 and from -191 to -292 mV/pCl$^-$ at pH 11. As the temperature of the solution was decreased, the dependence of E_{pit} on chloride concentration also decreased. For example, a slope of -129 mV/pCl$^-$ is observed at 95 °C, whereas -45 mV/pCl$^-$ was observed at 25 °C. When evaluated as a function of temperature, E_{pit} was found to increase with increasing temperature at low chloride concentrations (4.11 mV/°C at 3×10^{-4} M chloride) with an ever decreasing slope as the chloride concentration increased, so that at 5 M chloride the slope was -1.37 mV/°C. The dependence of E_{pit} on chloride concentration was also found to be a function of pH, with higher pH leading to greater dependence upon chloride.

Similarly, E_{rp} was observed to be dependent on the chloride concentration, but to a lesser extent than E_{pit}. The regression slopes ranged from -9 to -47 mV/pCl$^-$ at pH 9.5 and -40 to -118 at pH 11.0. Further, the regression coefficient (R^2) for E_{rp} was noticeably smaller under the same conditions than E_{pit}. The average R^2 for E_{pit} was 0.974 at pH 9.5 and it was 0.970 at pH 11.0. E_{rp}, on the other hand, had an average R^2 of 0.528 at pH 9.5 and 0.643 at pH 11. When evaluated as a function of temperature, E_{rp} was observed to generally decrease with increasing temperature at an average of -1.98 mV/°C independent of the chloride concentration with the exception of tests performed at 3×10^{-2} M chloride in which E_{rp} was found to slightly increase with temperature.

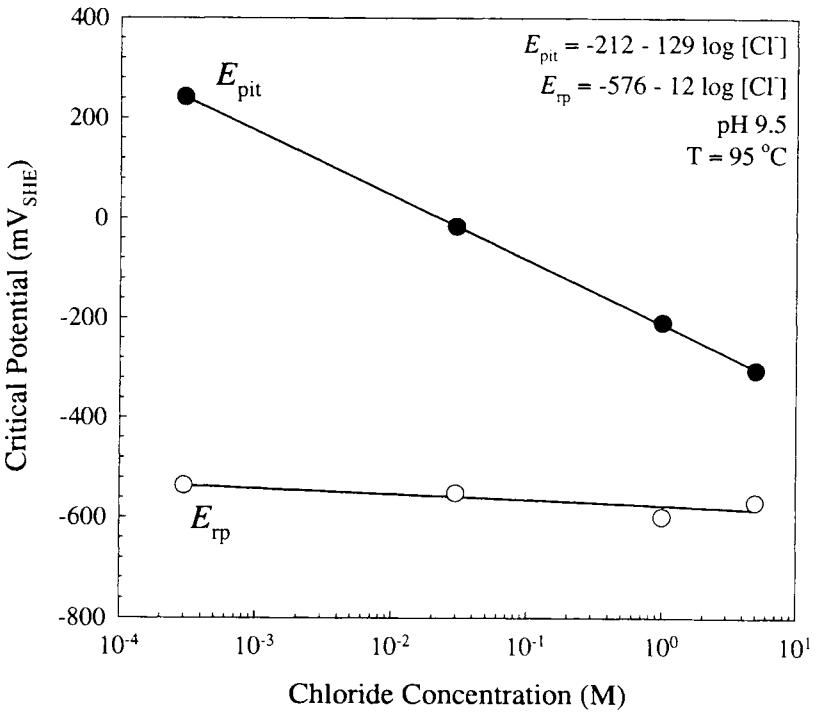

Figure 3-1. Effect of chloride concentration on E_{pit} and E_{rp} for A516 in HCO_3^-/CO_3^{2-} at pH 9.5 and 95 °C

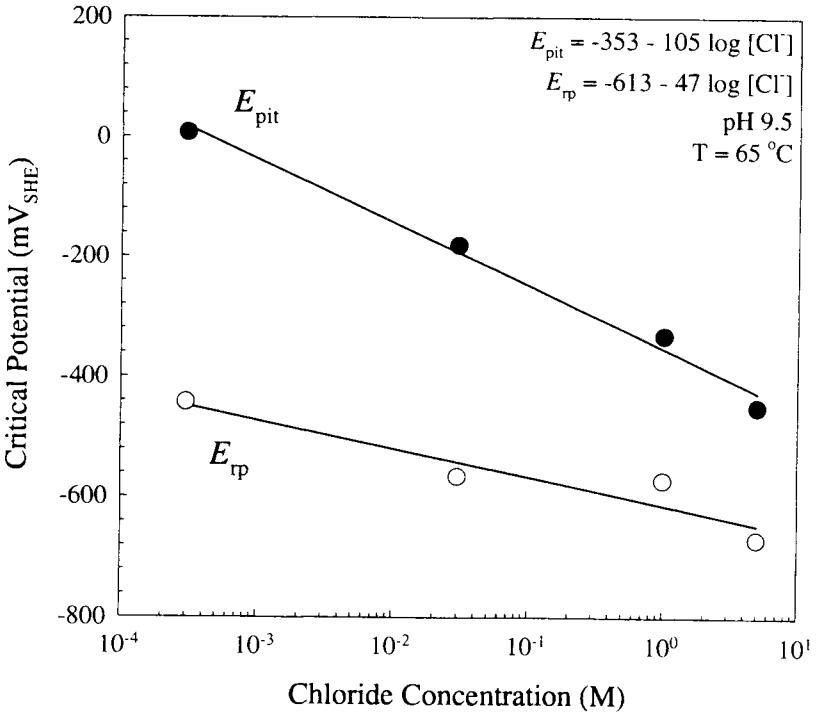

Figure 3-2. Effect of chloride concentration on E_{pit} and E_{rp} for A516 in HCO_3^-/CO_3^{2-} at pH 9.5 and 65 °C

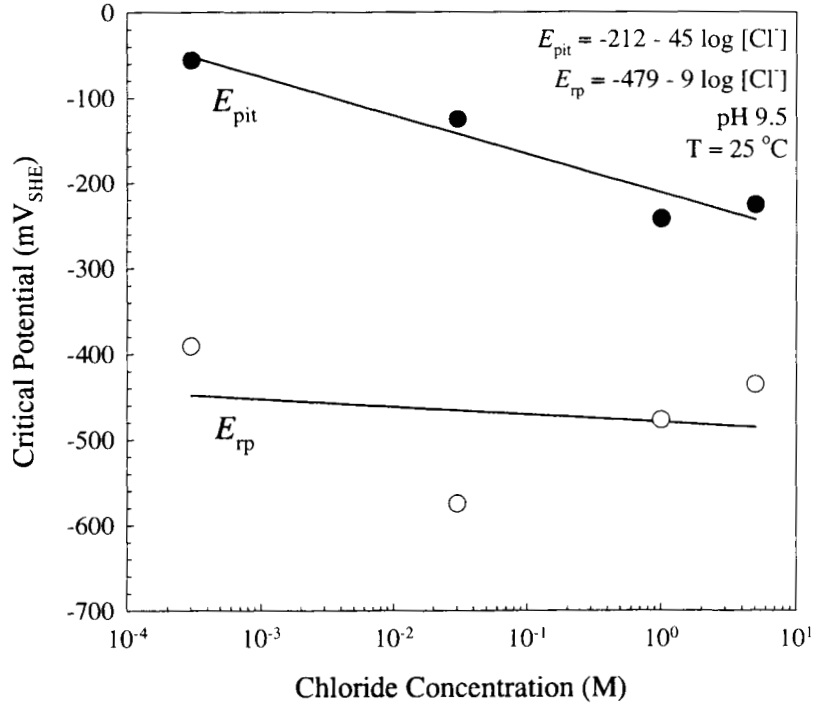

Figure 3-3. Effect of chloride concentration on E_{pit} and E_{rp} for A516 in HCO_3^-/CO_3^{2-} at pH 9.5 and 25 °C

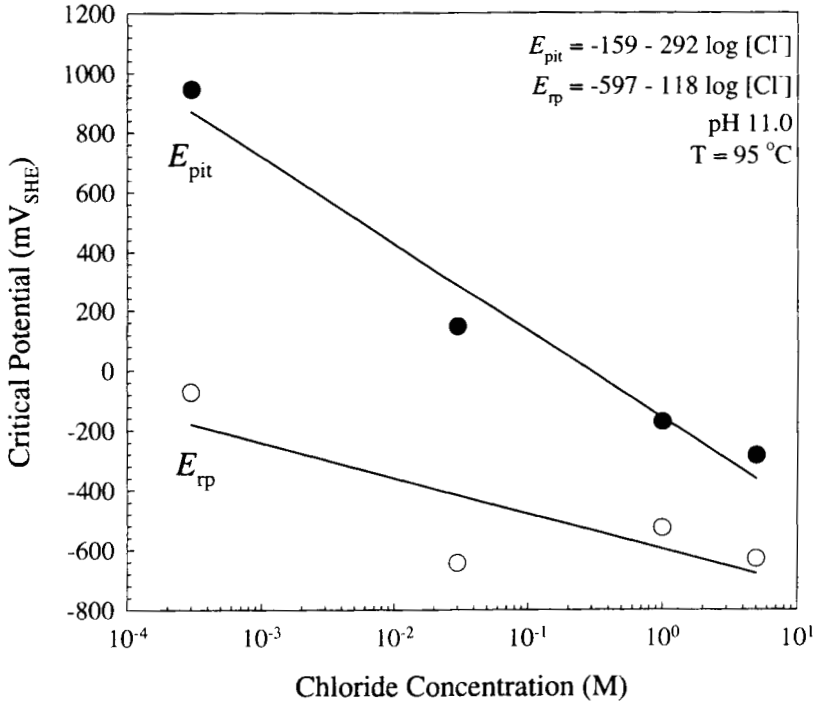

Figure 3-4. Effect of chloride concentration on E_{pit} and E_{rp} for A516 in HCO_3^-/CO_3^{2-} at pH 11.0 and 95 °C

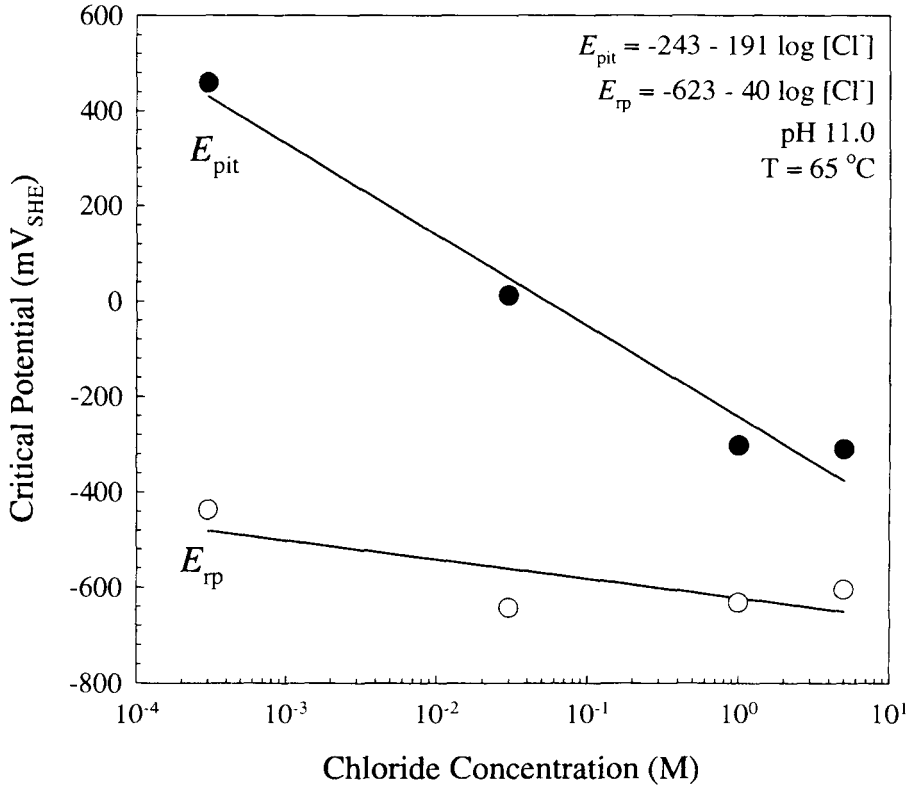

Figure 3-5. Effect of chloride concentration on E_{pit} and E_{rp} for A516 in HCO_3^-/CO_3^{2-} at pH 11.0 and 65 °C

3.1.2 Potentiostatic Pitting and Crevice Corrosion Tests

The effect of total carbonate concentration, chloride concentration, and temperature on pitting and crevice corrosion were evaluated using PP at potentials above the E_{rp} measured in CPP experiments. After testing, the samples were visually examined assigning a rating of severe, moderate, or minor pitting and general corrosion. Figure 3-6 shows the effects of the total carbonate:chloride ratio (ranging from 0.018 at 5×10^{-4} M CO_3^{2-} and 0.028 M Cl^- to 42.5 at 0.012 M CO_3^{2-} and 2.8×10^{-4} M Cl^-) and temperature (from 20 to 95 °C) on the extent and type of attack for cylindrical specimens polished to 600-grit finish. Note that the pH of the solution for these tests was 11.0. No clear pattern as to the dependence of the extent or type of attack on the carbonate chloride ratio or temperature was found. In fact, under nearly identical experimental conditions, moderate pitting corrosion and minor general corrosion were observed on different samples. When crevices were formed on the samples via pressing a serrated polytetrafluoroethylene (PTFE) disk onto the surface, the results became more consistent.

Figure 3-7 shows the effects of carbonate:chloride ratio (ranging from 0.425 at 0.012 M CO_3^{2-} and 0.028 M Cl^- to 42.5 at 0.012 M CO_3^{2-} and 2.8×10^{-4} M Cl^-) and temperature (at 20, 65, and 95 °C) on the extent of attack (at pH 11.0). Also shown in the figure are the weight loss measurements for each specimen in mg. As can be seen, the visual ranking and the quantitative weight loss measurements are in good agreement. Further, it is clear from the crevice testing that higher temperatures lead to greater corrosion. Additionally, decreased carbonate:chloride ratios also lead to increases in corrosion.

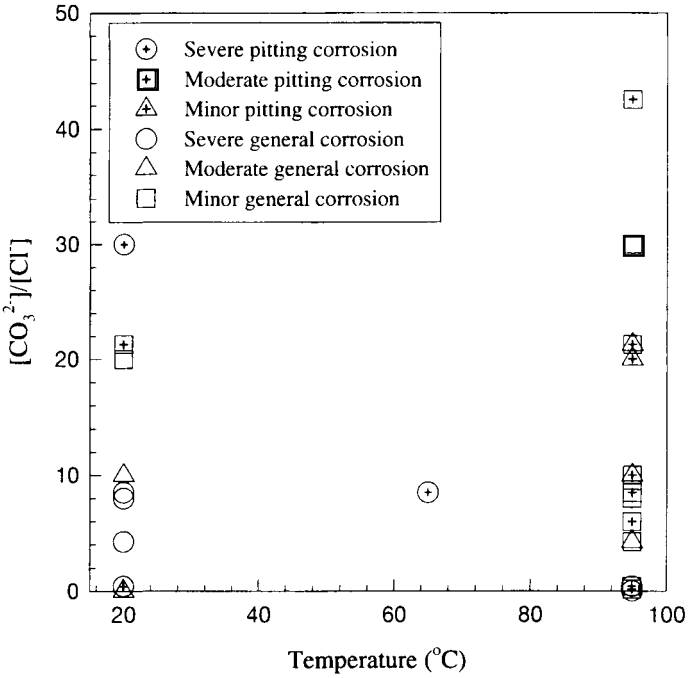

Figure 3-6. Effect of CO_3^{2-}/Cl^- ratio and temperature on the extent and type of corrosion observed after 24-hr potentiostatic tests on A516 above the E_{rp} measured from cyclic potentiodynamic polarization tests

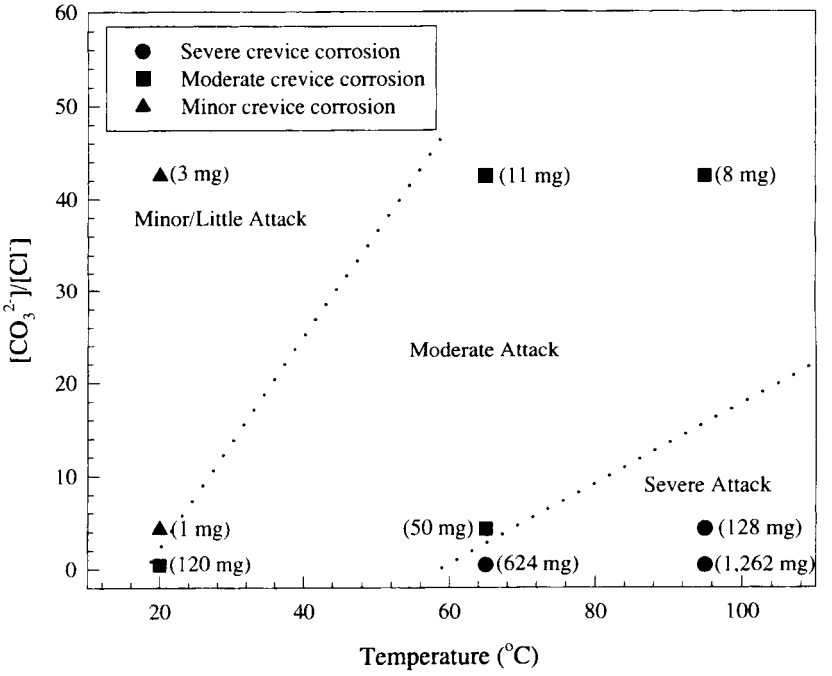

Figure 3-7. Effect of CO_3^{2-}/Cl^- ratio and temperature on extent of crevice corrosion attack observed during 24-hr potentiostatic tests on A516 held above the E_{rp} measured from cyclic potentiodynamic polarization tests. Also shown are the weight loss measurements for each specimen.

3.1.3 Experiments on Pit Stability and Growth

To evaluate the process governing pit stabilization of iron in chloride solutions, a LIP electrode made of 99.995 percent pure Fe was used. Use of high purity iron minimized voluminous generation of carbon dissolved in steel that obscured observation of chloride salt films. The electrode was polarized potentiostatically in deaerated 0.5 M HCl + 2 M NaCl. On polarization to +1.142 V_{SHE}, the current density increased to over 100 mA/cm^2. After an initial period of approximately 3 min during which the current density was nearly constant, the current density then began to decrease with time to 3–4 mA/cm^2, where it subsequently leveled off. This decrease in current density over time was found to be linear on a log-log plot with a slope of 0.5488, indicating the process is likely under mass transport control (a slope of 0.5 is indicative of mass transport controlled processes); that is, the diffusion of species through the salt film is controlling the dissolution rate. After approximately 500 min, a gel-like precipitate was observed in the glass sheath directly above the specimen.

The precipitate observed to form when the iron specimen was held at a constant applied potential of +1.142 V_{SHE} was characterized using *in situ* Raman spectroscopy. The *in situ* Raman spectra for the precipitate is shown in figure 3-8 along with the Raman spectra for $FeCl_2 \cdot 4H_2O$. It is evident from comparing the spectra for the precipitate and $FeCl_2 \cdot 4H_2O$ salt, that the precipitate is primarily composed of $FeCl_2$. Even though it appears that precipitation of an iron-chloride salt film has occurred in the simulated pit, and may be controlling the dissolution rate (as mentioned in the previous paragraph), the importance of salt film dissolution leading to pit repassivation and arrest is also an important key in determining pit stability.

To examine the effect of salt film precipitation and dissolution on the repassivation of the simulated 1D pit on iron, the precipitate was allowed to form and stabilize at +1.142 V_{SHE} overnight (over 16 hr). The applied potential was then systematically decreased in 0.45 V increments and the current response monitored (figure 3-9). Each decrease in potential resulted in an instantaneous decrease in the current, which rapidly increased back to its original value. This behavior was observed at potentials as low as -0.208 V_{SHE}, where after the decrease to this low potential the current remained relatively high after the initial decrease even though this potential is approximately 200 mV above the open circuit potential for the iron electrode in this system. At this low potential, the salt film was no longer visually observable.

3.2 LOCALIZED CORROSION OF NI-BASE CORROSION RESISTANT MATERIALS

3.2.1 Effect of Groundwater Chemistry on the Localized Corrosion of Ni-Base Materials

The effects of chloride concentration on E_{pit} and E_{rp} of Alloy 825 (figure 3-10), as measured in CPP tests have been discussed previously (Sridhar et al., 1995) and are presented here for completeness. The E_{pit} and E_{rp} are measured in deaerated environments so that a large potential range can be investigated without interference with the oxygen reduction reaction. Although the presence of oxygen is not expected to alter the values of E_{pit} and E_{rp}, the kinetics of the oxygen reduction reaction may determine the corrosion potential of the container materials in a repository environment. Hence, corrosion potential data in air-saturated environments are also shown in figure 3-10. It is apparent that both E_{pit} and E_{rp} are strongly dependent on the concentration of chloride. At chloride concentrations less than 10^{-3} M, the E_{pit} and the E_{rp} are almost identical. Pitting did not occur in all the specimens tested in low chloride concentration solutions. Where

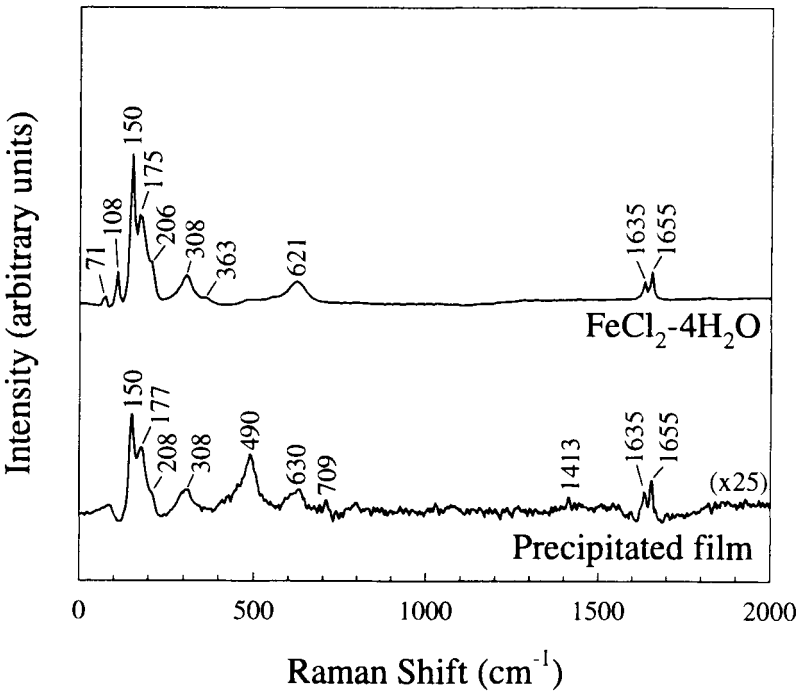

Figure 3-8. *In situ* Raman spectra of the precipitated gel-like salt film formed in one-dimensional simulated pit on iron and Raman spectra for $FeCl_2 \cdot 4H_2O$ salt standard. Note that the intensity of the film spectra has been multiplied by a factor of 25 to enable viewing on a similar scale with the salt standard.

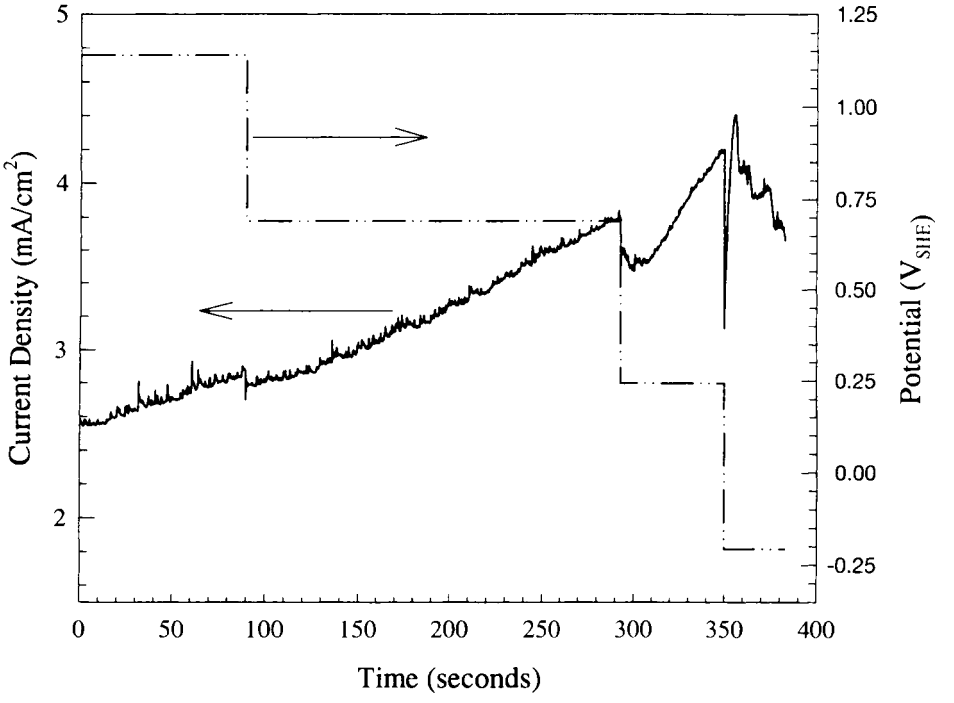

Figure 3-9. Effect of systematically decreasing the potential after formation of a salt film in a one-dimensional simulated pit on iron

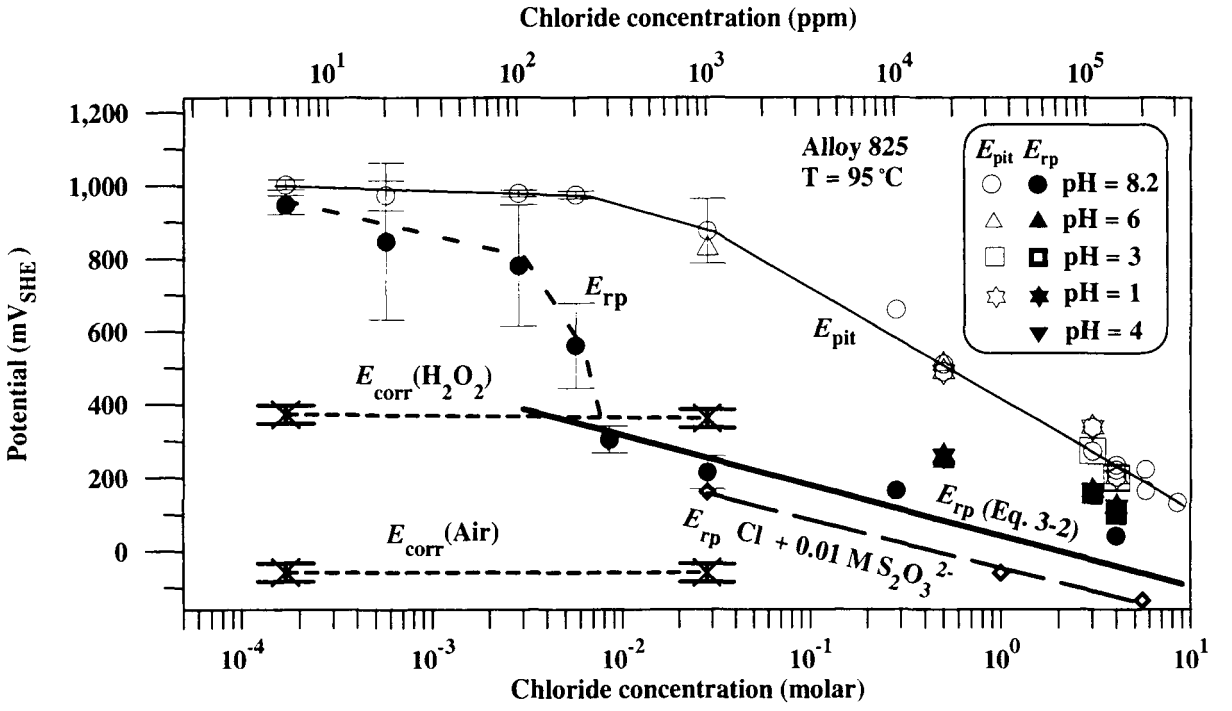

Figure 3-10. Critical potentials for localized corrosion initiation and repassivation of Alloy 825 as a function of chloride concentration and solution pH. Regression line for E_{rp} data from cyclic potentiodynamic polarization tests is indicated. Corrosion potentials measured after 30 min exposure.

pitting did not occur, the E_{rp} has no physical meaning. The high E_{pit} value represents the potential at which the oxygen evolution reactions occurs on the alloy surface. The net result of the hysteresis in this reaction is a large scatter in the data at chloride concentrations less than 10^{-2} M. At chloride concentrations in the range of 10^{-2} to 1 M, a large difference between E_{pit} and E_{rp} is observed. The critical potentials for Alloy 825 are higher than those for type 316L stainless steel (SS), especially at low chloride concentrations (Dunn et al., 1997). The difference between these potentials, however, is significantly reduced at high chloride concentrations. Another notable observation is the relative independence of E_{rp} with pH over a wide pH range. This observation is consistent with the current understanding of the pitting process where the pH inside the pit is dictated by the hydrolysis of cations and becomes independent of the external pH.

An expression for E_{rp} in temperature and chloride concentration over the range of 10^{-3} to 9 M (pH 1 to 8.2) was obtained by using the lowest measured value of E_{rp} for each chloride concentration as a conservative criterion to predict the initiation and repassivation of localized corrosion (Mohanty et al., 1997). The general expression for E_{rp} is given in Eq. (3-2), with specific parameters for Alloy 825 over the Cl^- concentration range of 10^{-3} to 9 M in Eq. (3-3):

$$E_{rp} = E^0_{rp} + B(T)\log[Cl^-] \tag{3-2}$$

$$E^0_{rp}(T) = 428.2 - 4.1(T); \quad B(T) = 64.0 - 0.8(T) \tag{3-3}$$

where, E_{rp} in mV_{SHE} is the repassivation potential for localized corrosion (pitting and crevice corrosion), and E_{rp}^{0} (T) in mV_{SHE} is the repassivation potential at 1 M chloride concentration Eq. (3-2). Previous work established the dependence of E_{rp} on other environmental factors such as the concentrations of NO_3^-, SO_4^{2-}, and F^- (Cragnolino and Sridhar, 1991). As shown in figure 3-10, thiosulfate ($S_2O_3^{2-}$) decreases the E_{rp} significantly. The effect of $S_2O_3^{2-}$ observed in this study is similar to that found by Nakayama et al. (1993).

The effect of chloride concentration on the crevice repassivation, E_{crev} and initiation potentials, E_{rcrev}, of Alloy 625 at 95 °C is shown in figure 3-11. Crevice corrosion specimens were used exclusively as a result of the inconsistent formation of localized corrosion pits on cylindrical specimens of Alloy 625 during CPP tests. For the crevice corrosion data shown in figure 3-11, the potential that resulted in a pronounced increase in current density in the forward portion of the CPP scan was taken to be E_{crev} and the potential at the point where the forward and reverse scans intersect was taken as E_{rcrev}. The extent of the investigation of localized corrosion of Alloy 625 was limited compared to Alloy 825. The data shown in figure 3-11 were all obtained at 95 °C (Gruss et al., 1998). Because of the limited number of tests, the best fit line for the E_{rcrev} values shown in figure 3-11 and represented by Eq. (3-4) is only valid for 95 °C

$$E_{rcrev} = 98.6 - 160.8\log[Cl^-] \tag{3-4}$$

where E_{rcrev} is in mV_{SHE}. Eq. (3-4) is limited to the concentration range of 0.1 to 11 M chloride. At lower chloride concentrations the value of the E_{rcrev} increases to potentials above 540 mV_{SHE}. In addition significantly more scatter is observed with E_{rcrev} measurements made at chloride concentrations less than 0.1 M. Increasing the chloride concentration to values above 0.1 M results in a decrease in both the measured values of E_{rcrev} and the dispersion of the data. Similar behavior was also observed on Alloy 825 specimens in solutions where the chloride concentration was greater than 0.01M.

Crevice corrosion of Alloy C-22 was also investigated by the CPP method (Gruss et al., 1998). A test solution containing a 4 M of chloride ion concentration at 95 °C and an initial solution pH of 2.5 produced a small region of crevice corrosion on one of the creviced specimens. A small hysteresis loop was observed in the CPP data for this specimen. The crevice initiation potentials measured on this specimen was 855 and the repassivation potential was 825 mV_{SHE}. No crevice corrosion was initiated in the CPP tests performed in solutions containing less than 4 M chloride, although well defined hysteresis loops were often observed. The initiation of pitting corrosion on cylindrical specimens was not observed during CPP tests in solutions containing less than 4 M chloride. The CPP scan shown in figure 3-12 is for a cylindrical CPP specimen tested in 4 M chloride at 95 °C. In spite of the well defined hysteresis, no pitting was initiated on the test specimen.

Using the LIP specimen geometry, the E_{rp} of single simulated pits was measured (Gruss et al., 1998). These tests were performed in solutions containing up to 4 M chloride. Initiation of pitting corrosion was accomplished by maintaining the potential of the test specimens above 1.2 V_{SHE} for a period of at least 10 hr. Active dissolution inside the simulated pit was confirmed by both the anodic current densities in excess of 10^{-3} A/cm^2 and a green corrosion product inside the simulated pit. Measured values for the E_{rp} of single pit Alloy C-22 specimens are shown in figure 3-13. Lines for the E_{pit} and E_{rp} of Alloys 825 and 625 are also shown in order to compare the performance of the three alloys. It is evident from this figure that Alloy 825 is the poorest performing alloy. Alloy 625 performed better than Alloy 825 at low chloride concentrations,

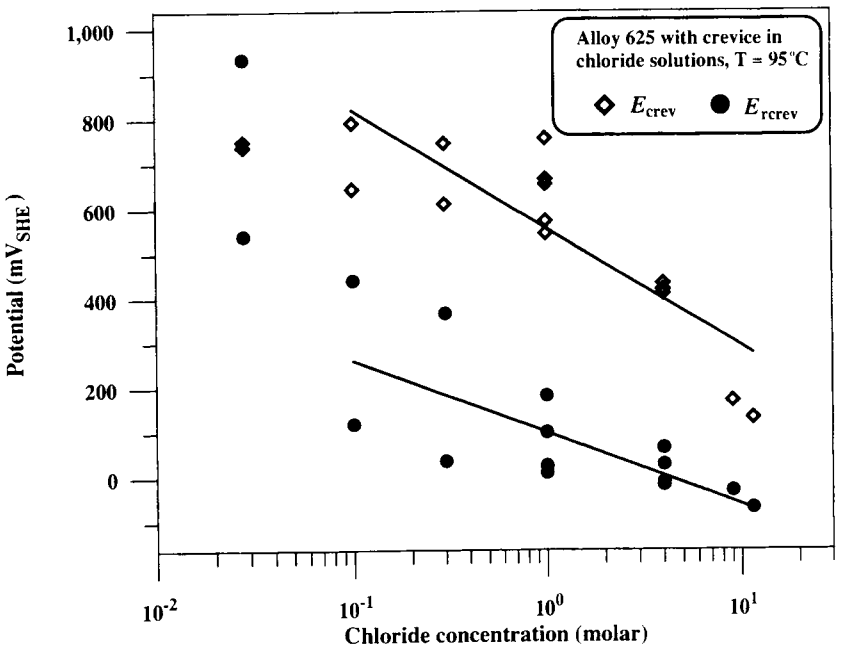

Figure 3-11. Critical potentials for localized corrosion initiation and repassivation of Alloy 625 as a function of chloride concentration. Regression line for E_{rp} data from cyclic potentiodynamic polarization tests is indicated.

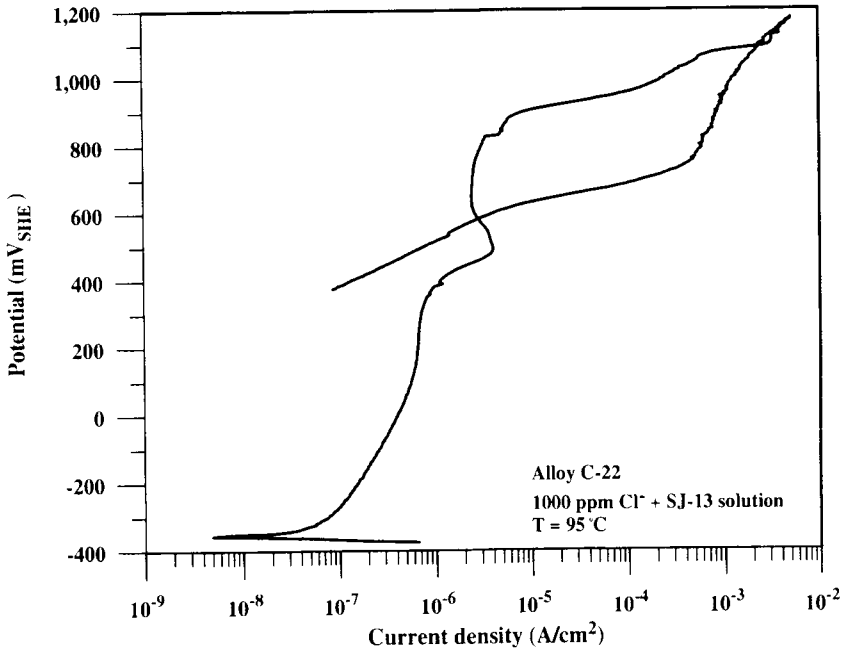

Figure 3-12. Cyclic potentiodynamic polarization curve of Alloy C-22 in a 1,000 ppm chloride solution at 95 °C. Although a significant hysteresis is apparent, no localized corrosion of the specimen was observed.

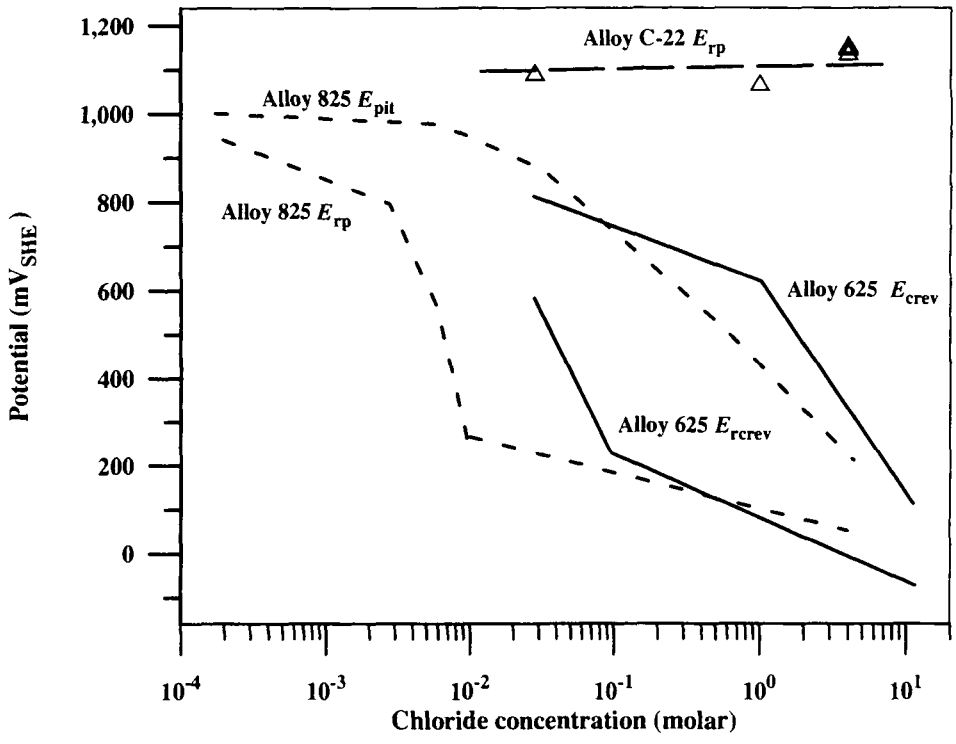

Figure 3-13. Critical potentials for Alloys 825, 625, and C-22. Alloy 625 data obtained with creviced specimens. Alloy C-22 data obtained with lead-in-pencil specimens.

however, at chloride concentrations above 0.1 M the performance of Alloys 625 and 825 is very similar. In contrast, the E_{rp} of Alloy C-22 is greater than 900 mV_{SHE} at chloride concentrations in the range of 0.02 to 4 M. The high values of E_{rp} and the low dependence on chloride concentration indicates that Alloy C-22 is extremely resistant to localized attack in oxidizing chloride solutions.

3.2.2 Long-Term Testing of Alloy 825

The use of the E_{rp} as a parameter to predict the onset of localized corrosion has been evaluated in long-term (up to 1,400 days) testing where Alloy 825 specimens were maintained at potentials either above or below E_{rp} (Dunn et al., 1996). The effect of applied potentials as well as corrosion potentials under various redox conditions on the time to initiate localized corrosion is shown in figure 3-14. At potentials near the E_{pit} measured in CPP tests (e.g., 840 mV_{SHE}), the initiation time was on the order of 200 sec. Decreasing the potential to 740 mV_{SHE} resulted in initiation times of 200,000 sec. In contrast, relatively short initiation times for crevice corrosion were observed even at applied potentials several hundred millivolts below E_{pit}. Figure 3-14 also shows pitting and crevice corrosion initiation times for specimens at open-circuit potentials under various redox conditions such as 1,000 ppm (0.028 M) chloride with a Cu^{2+}/Cu^{+} redox couple. The error bands in these data points denote the variation in the corrosion potentials for the same redox couple used. No pitting corrosion was observed on the boldly exposed surfaces (i.e., the surface of the specimen not covered with a crevice former) of any of the creviced specimens. In addition, no pitting corrosion was observed on a boldly exposed specimen in which the open-circuit potential was in the range of

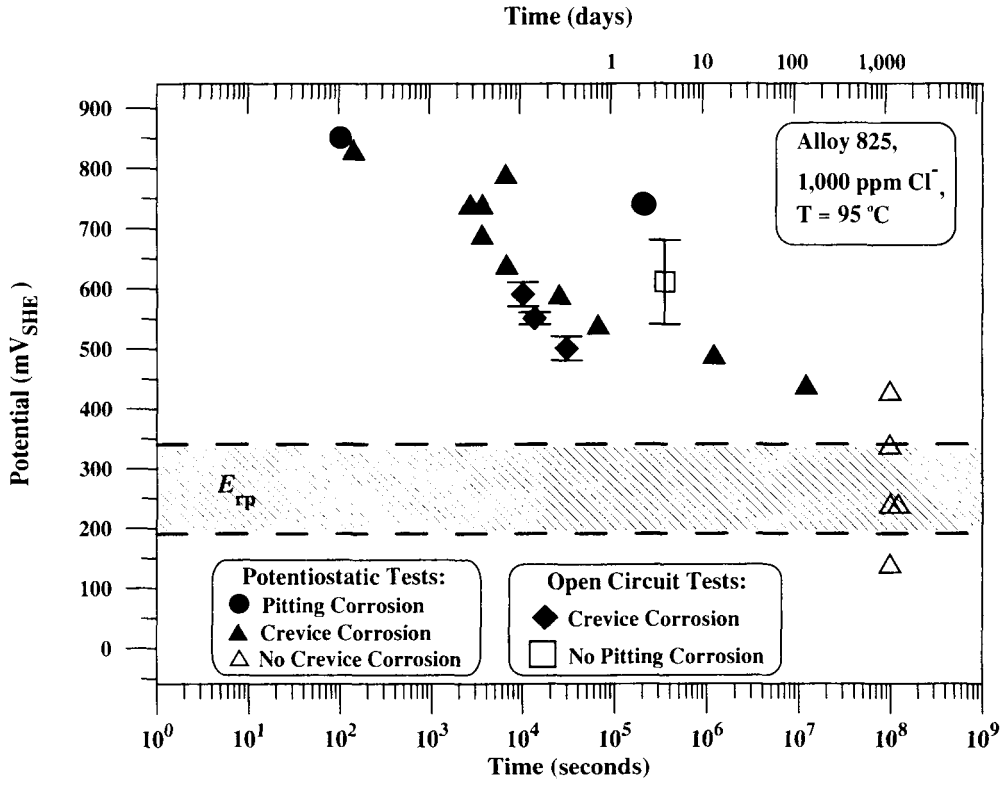

Figure 3-14. The effect of applied and corrosion potentials under various redox conditions on pitting and crevice corrosion initiation times for Alloy 825 in a 1,000 ppm chloride solution at 95 °C

540–680 mV_{SHE}. It is clear that the initiation time for pitting and crevice corrosion under natural exposure conditions is consistent with that under applied potential conditions. Tests are continuing to further evaluate this observation.

While the long-term potentiostatic tests provide strong evidence for the use of E_{rp} as a parameter to predict the minimum potential at which localized corrosion can be initiated, it is clear that the environmental conditions within the repository will determine if localized corrosion of the inner corrosion resistant barrier can occur. Since localized corrosion can only be initiated at potentials above E_{rp}, it follows that predictions of container performance can only be made with knowledge of the E_{corr} of the material in the environment of interest. A long-term measurement of the corrosion potential of creviced Alloy 825 specimens in a 1,000 ppm (0.028 M) chloride solution is shown in figure 3-15. Initially the corrosion potential was about -160 mV_{SHE}, which is well below the repassivation potential. Over time the mill finished surface of the specimen in which Cr depletion has been detected, was corroded away leaving behind material with the bulk chromium composition (Dunn et al., 1995). The improved passive film decreases the anodic dissolution rate that results in an increased E_{corr}. After 300 days of testing the E_{corr} was greater than the E_{rp}. Examination of the specimen after 500 days revealed areas of crevice corrosion that occurred only when the E_{corr} was greater than the E_{rp}. Continued testing resulted in a sudden decrease in the E_{corr} after 850 days of testing. This decrease was followed by an increase in E_{corr} that eventually reached potentials as high as 540 mV_{SHE}.

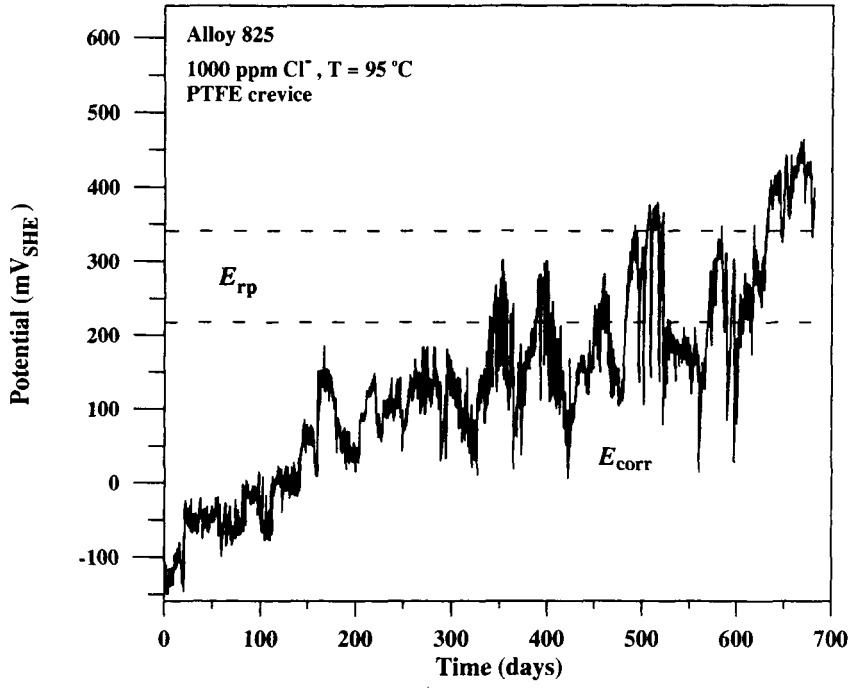

Figure 3-15. Evolution of the corrosion potential of Alloy 825 exposed to a 1,000 ppm chloride solution at 95 °C. Crevice corrosion was observed only when E_{corr} exceeded E_{rp}.

3.2.3 Galvanic Coupling on Container Materials

The effect of galvanic coupling of the WP materials on the overall performance of the containers has been examined by calculating the expected corrosion potentials of the WP materials and conducting laboratory testing (Dunn and Cragnolino; 1997, 1998). Calculations of the corrosion potential of an Alloy 825 inner barrier galvanically coupled to a perforated A516 steel outer barrier indicated that the inner Alloy 825 barrier should exhibit E_{corr} much lower than the E_{rp}. Galvanic corrosion tests where the Alloy 825 specimens were coupled to A516 steel through a zero resistance ammeter largely confirmed the calculated values of the galvanic corrosion potentials. The effects of environmental variables and material area ratios were found to be small. As expected, higher values of E_{corr} were observed in high pH, aerated solutions where the area of Alloy 825 was greater than the A516 steel area. Under all conditions tested, however, the E_{corr} of Alloy 825 when directly coupled to A516 steel was at least 400 mV less than the E_{rp} for Alloy 825.

To initiate localized corrosion of the Alloy 825 inner barrier, the efficiency of the galvanic coupling between the container barriers must be reduced such that the E_{corr} of the Alloy 825 inner barrier exceeds the E_{rp} (Dunn and Cragnolino, 1997; 1998). The geometry of the double barrier WP consisting of an inner Alloy 825 barrier and an outer A516 steel barrier should result in a galvanic coupling efficiency adequate for protecting the inner barrier from localized corrosion.

Formation of oxide scales and corrosion product layers between the WP barriers may decrease the galvanic coupling efficiency. Evaluation of the effects of inefficient galvanic coupling between Alloy 825 and A516 steel was conducted by measuring the corrosion potential of the two materials under a range of

coupling conditions and environments (Dunn et al., 1998). Figure 3-16 shows the corrosion potential measurements for both Alloy 825 and A516 steel in an aerated 1,000 ppm chloride solution at 95 °C. When the solution pH is acidic the corrosion potential of the two materials is in the range of -350 to -400 mV_{SHE}. Even though the corrosion potentials of the bimetallic couples increases with pH, the potential difference between the coupled specimens, however, was limited to a few millivolts. No localized corrosion was initiated on any of the Alloy 825 specimens. In the pH 3 solution, A516 steel suffered nonuniform general corrosion. Large regions of unattacked areas and numerous small pits were observed on A516 steel specimens tested in pH 8 and pH 10.8 chloride solutions. In most cases the pits in the A516 steel specimens were 10–50 μm deep.

Corrosion potentials of uncoupled Alloy 825 and A516 steel, obtained by immersing the two materials in a 1,000 ppm chloride solution at pH 3, are shown in figure 3-17. The E_{corr} of Alloy 825, measured to be between 150 to 250 mV_{SHE}, tended to increase with time. Although the E_{corr} of this specimen was near the lower bound of the E_{rp} for Alloy 825, post-test examination of the specimen did not reveal any indication of localized corrosion. The E_{corr} of the polished A516 steel specimen was in the range of -420 to -480 mV_{SHE}. Galvanic coupling of the two materials performed with the mill scale of A516 steel left intact results in an increase in the E_{corr} of A516 steel to -420 to -380 mV_{SHE}. Although the mill scale was left intact, the E_{corr} of Alloy 825 was significantly reduced as a result of highly efficient galvanic coupling to the A516 specimen. Initially the E_{corr} of Alloy 825 was -210 mV_{SHE}. Within a few hr, the E_{corr} of the Alloy 825 specimen was reduced to a E_{corr} close to that of the A516 steel specimen.

The corrosion potentials of Alloy 825 and A516 steel specimens tested with a 1.5 mm thick layer of possible corrosion products separating the materials are shown in figures 3-18 and 3-19. When the two materials were coupled through a layer of corrosion products from A516 steel, the E_{corr} was very similar to the uncoupled specimen. Similar results were obtained when the specimens were coupled through 1.5 mm thick layers of γ-FeOOH or α-Fe_2O_3. Again, no evidence of localized corrosion was observed. Several tests were performed with the two materials coupled through a 1.5 mm thick layer of reagent grade Fe_3O_4. Large variations in the E_{corr} of Alloy 825 were observed under these conditions. The E_{corr} of Alloy 825 coupled to A516 steel through Fe_3O_4 in figure 3-18 represents the median in the range of E_{corr} values observed. In this test, the E_{corr} was initially above 0 V_{SHE}. Over a period of several days, the potential decreased and varied in the range of -200 to 0 mV_{SHE}. During the latter stages of the test the E_{corr} decreased substantially to values near -400 V_{SHE} and a corresponding increase in the E_{corr} of A516 was observed. Additional tests performed under identical conditions resulted in E_{corr} of Alloy 825 similar to an uncoupled specimen and, in another case, similar to an Alloy 825 specimen that was efficiently coupled to A516 steel (Dunn et al., 1998). In all cases, however, initiation of localized corrosion on Alloy 825 was not observed.

The results obtained when A516 steel specimen was coupled to Alloy 825 through a 1.5 mm thick layer of $FeCl_3$ are shown in figure 3-19. Although the E_{corr} of Alloy 825 measured in the latter portion of this test was only slightly higher with respect to the uncoupled condition, numerous small pits up to 30 μm deep were observed at the conclusion of the test. Some pitting was also observed on the A516 steel specimen, however, the majority of the attack was in the form of general corrosion. The E_{corr} of Alloy 825 coupled through β-FeOOH to A516 steel is also shown in figure 3-19. Initially the E_{corr} was greater than 400 mV_{SHE}. A decrease in the E_{corr} to values around 300 mV_{SHE} were observed after approximately 1 day of testing. After several days of slowly decreasing from 300 mV_{SHE}, the E_{corr} underwent large fluctuations before stabilizing in the range of -300 to -200 mV_{SHE}.

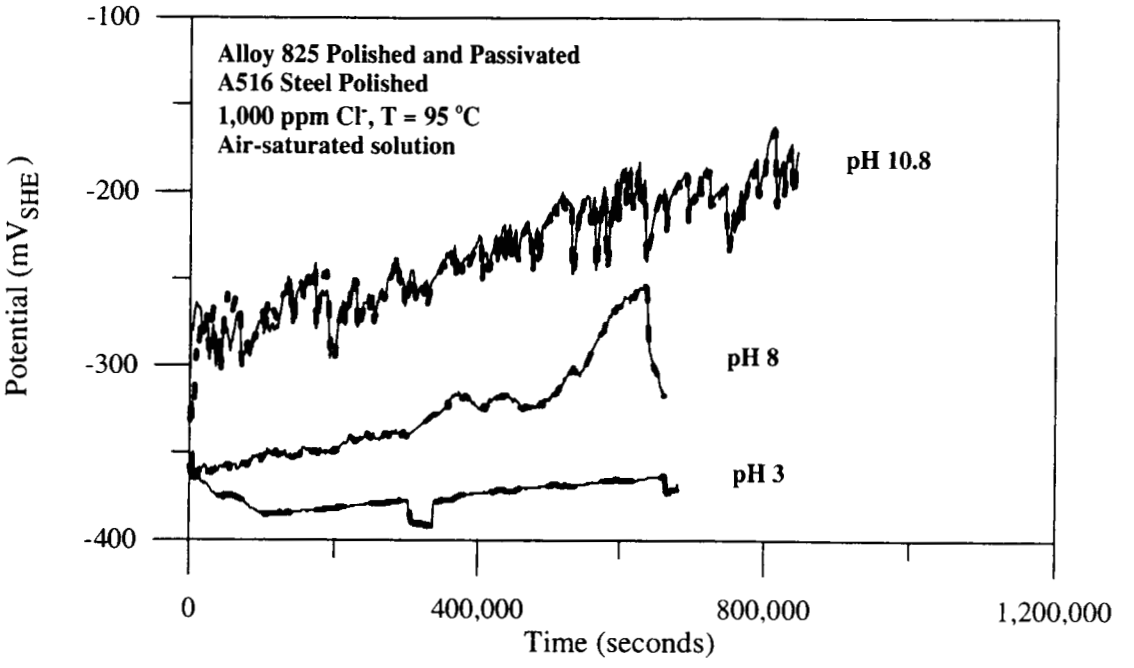

Figure 3-16. Galvanic corrosion potentials of Alloy 825 coupled to A516 steel in air-saturated 1,000 ppm chloride solution

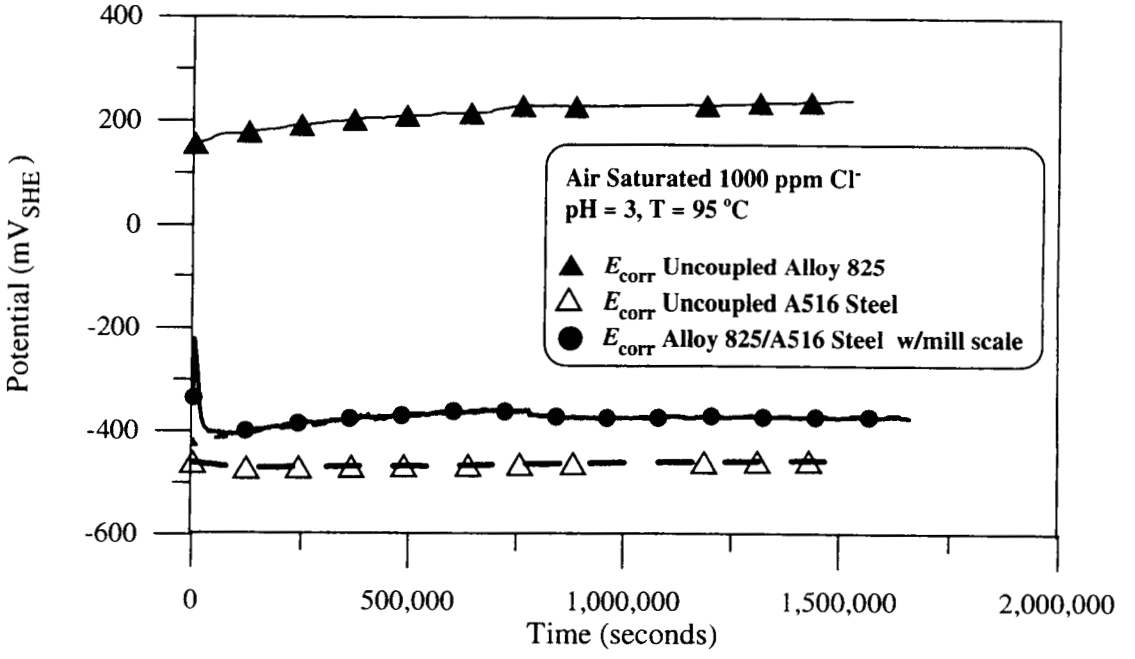

Figure 3-17. Corrosion potentials of coupled and uncoupled Alloy 825 and A516 steel in air-saturated 1,000 ppm chloride solutions adjusted to pH 3. A516 steel specimens tested with mill scale.

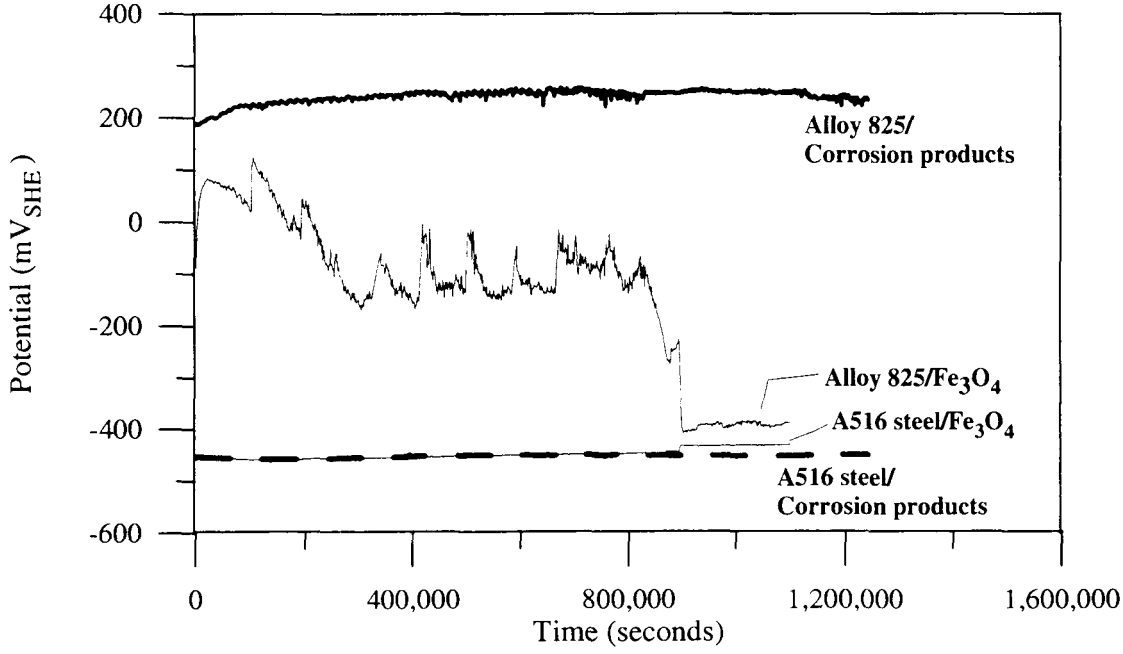

Figure 3-18. Galvanic corrosion potentials of Alloy 825 and A516 steel couples exposed in a 1,000 ppm chloride solution at pH 3. Specimens were separted with a 1.5 mm thick O-ring filled with Fe_3O_4 or A516 steel corrosion products.

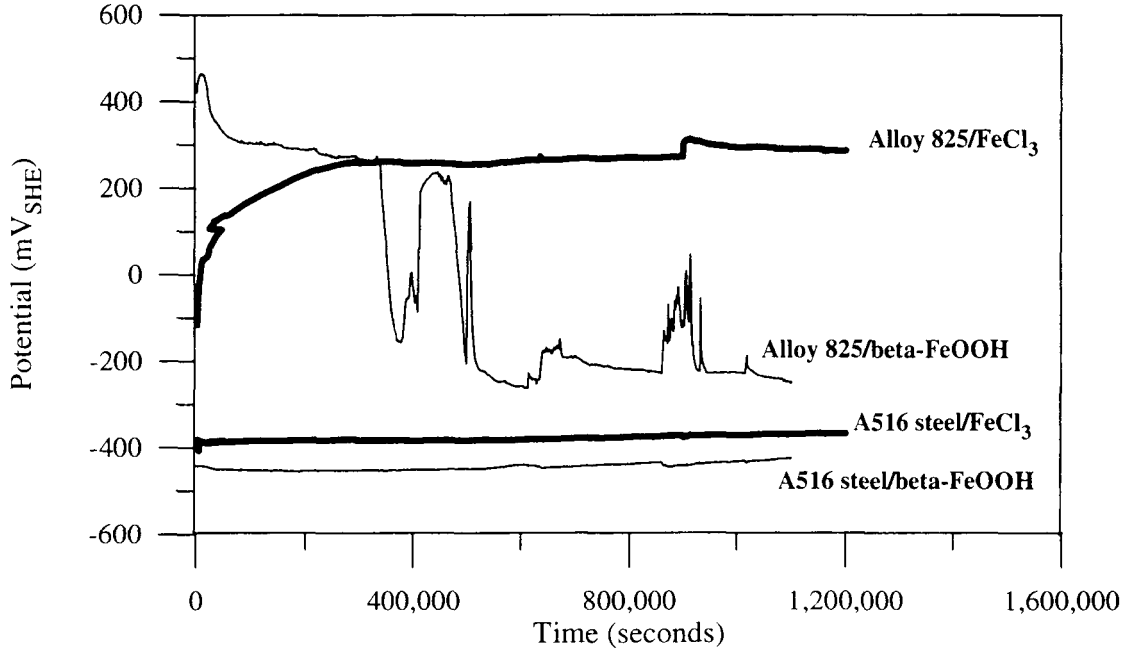

Figure 3-19. Galvanic corrosion potentials of Alloy 825 and A516 steel couples exposed in a 1,000 ppm chloride solution at pH 3. Specimens were separted with a 1.5 mm thick O-ring filled with $FeCl_3$ or β-FeOOH.

4 DISCUSSION

4.1 EFFECT OF ENVIRONMENT ON PITTING AND REPASSIVATION POTENTIALS

4.1.1 Effect of Environment on Pitting and Repassivation Potentials

Localized corrosion of carbon steel is a complex function of environmental conditions. In the present work, the pitting behavior of A516 carbon steel was examined potentiodynamically in mixed carbonate/bicarbonate solutions of varying chloride concentration and temperature. The total carbonate concentration was kept constant at 0.012 M, but the ratio of HCO_3^-/CO_3^{2-} was varied to obtain pH values of 9.5 and 11. From these experiments, the critical potentials (pitting potential, E_{pit}, and repassivation potential, E_{rp}) were determined. The pitting potential represents the driving force necessary for pit nucleation and growth on a given material in a given environment. The repassivation potential represents the minimum potential for pit nucleation to occur for a given specimen in a given environment, below which no pitting takes place and any pits already present are arrested and cease propagating. Pitting on carbon steels can nucleate on a number of different sites including metal sulfide inclusions, mixed metal sulfide-oxide particles, grain boundaries, and oxide particles (Szklarska-Smialowska, 1986). This report does not address the nature of sites of localized corrosion nucleation, but a distinction is drawn here to note the differences between localized corrosion of carbon steels and pure iron, for which a considerable body of literature exists and will be used as a basis for comparison of the results of the present work. Because iron does not have the heterogeneities present in carbon steels that act as preferential sites for localized corrosion, iron will generally exhibit greater resistance to localized corrosion than carbon steel.

The E_{pit} and E_{rp} were evaluated in the present work as a function of chloride concentration (3×10^{-4} to 5 M) and temperature (25, 65, and 95 °C). Both E_{pit} and E_{rp} were found to have a logarithmic dependence on chloride concentration of the form shown in Eq. (3-1). The regression slopes for E_{pit} and E_{rp} for the conditions studied are shown in table 4-1. The values for the slope for the present study are in agreement with those reported in the literature of between 60 and 200 mV/pCl$^-$ (Szklarska-Smialowska, 1986; Alvarez and Galvele, 1984). The high slope of 292 mV/pCl$^-$ observed for E_{pit} at pH 11 and 95 °C is likely due to delayed initiation at low chloride concentrations. For example, if the data point associated with 2.8×10^{-3} M chloride was removed and the regression analysis performed, the regression slope then becomes 196 mV/pCl$^-$. Further, the minimum chloride concentration reportedly required for localized corrosion of iron to occur is on the order of 0.3×10^{-4} to 3×10^{-3} M in acidic to slightly alkaline buffer solutions (Szklarska-Smialowska, 1986), which is in line with the minimum chloride concentration examined here. In contrast to E_{pit}, E_{rp} has generally been observed to be independent of chloride concentration (Sussek and Kesten, 1975). In the present case, the values of B for E_{rp} were in the range of 9 to 47 at pH 9.5 and 40 to 118 at pH 11.0, thus, at least under some circumstances, exhibiting a strong dependence on the chloride concentration. One possible explanation for this is that the method by which E_{rp} was measured in the present case is dependent on the depth of pitting on the surface depth prior to repassivation. Thus, more extensive pitting prior to repassivation would result in a lower E_{rp}. Alvarez and Galvele (1984) however, have shown using scratch repassivation tests on pure iron that E_{rp} is dependent on chloride concentration, thus changes in the extent of pitting may not be responsible for the observed dependence of E_{rp} on chloride concentration. Another possible explanation for observed dependence of E_{rp} on chloride concentration could be related to the stability of pits and the critical chloride concentration required to achieve nucleation.

Table 4-1. Effect of temperature and pH on the gradient, B, for E_{pit}

pH	B in Eq. (3-1) for E_{pit}			B in Eq. (3-1) for E_{rp}		
	95 °C	65 °C	25 °C	95 °C	65 °C	25 °C
9.5	129	105	45	12	47	9
11.0	292	191	n/a	118	40	n/a

E_{pit} and E_{rp} were also found to depend on the pH of the solution, with the value of E_{pit} increasing by an average of 55 mV/pH and E_{rp} decreasing by an average of -10 mV/pH. Further, the slope of E_{pit} with chloride concentration also changed with pH, as can be seen in table 4-1. Several researchers have observed for pure iron in chloride solutions a lack of dependence of E_{pit} on pH in the range of 8 to 12.7 (Szklarska-Smialowska, 1986). Other studies on iron and on carbon steels, however, have shown a marked dependence of E_{pit} on pH, changing by 20–125 mV/pH (Alvarez and Gavele, 1984; Simard et al., 1998) above a pH of 10. The observed increase in the pitting potential on increasing the pH shows that increasing the pH has somewhat of an inhibiting effect for carbon steel in chloride solutions. The slight decrease in E_{rp} with pH seems to indicate that pit arrest would be more difficult at higher pH. In the present case, however, the dependence of E_{rp} on pH is relatively small, and given the scatter in the E_{rp} data, may be an experimental artifact.

Numerous mechanisms have been proposed to explain the role of chloride on the pitting of iron and carbon steels (Szklarska-Smailowska, 1986; Simard et al., 1998). From the work in this study, it is not clear which mechanism is operable, but some of the phenomena observed can be explained by invoking the hypothesis that one of the required steps for pitting to occur is adsorption of chloride onto the metal surface. For example, the increase in E_{pit} observed upon increasing the pH in reality should be examined as a case in which the overall CO_3^{2-} concentration increased. As such, for a given chloride concentration, increases in the CO_3^{2-} concentration would lead to increases in E_{pit} via competitive migration and adsorption processes. This has been experimentally observed and theorized by others. Simard et al. (1998) proposed that pitting of iron in chloride solutions results from adsorption of chloride on the metal surface that then forms cation complexes (e.g., $FeCl^+$) inducing film dissolution and thinning. The chloride eventually reaches the metal surface, at which point rapid dissolution occurs. Increasing the pH via increases in the CO_3^{2-} concentration (as was done here) had an inhibitive effect (E_{pit} increased) via competitive adsorption with chloride, similar to OH^-, which is known to promote passivation (Szklarska-Smialowska, 1978). Others have proposed that when iron was exposed to HCO_3^-/CO_3^{2-} solutions, a Fe_3O_4 film was formed with chloride acting to catalytically liberate Fe^{3+} from the film and induce breakdown (Mao et al., 1994). Bird et al. (1988) redefined the relationship between E_{pit} and chloride concentration to include the concentration of OH^-, which acted as a pit inhibitor. Thus, although it is unclear specifically by what mechanism pitting is taking place on A516 steel, the likely explanation for the improved performance at higher pH in the present case is because of increased CO_3^{2-} concentration, which acts as a pitting inhibitor. In the absence of carbonate, changes in the pH have generally been observed to have negligible effects on E_{pit} (Szklarska-Smailowska, 1986).

Another possible explanation for the role of chloride on the pitting of metals that should also be considered involves the critical solution chemistry required for localized corrosion initiation and propagation. It is well established that the development and maintenance of a critical occluded site solution chemistry is required for localized corrosion (Frankel, 1998). Further, the maintenance of this solution chemistry during

pitting corrosion is often thought to be aided through the development of a covering (e.g., precipitation of a salt film or remnants of the passive oxide) or because of the presence of a second phase particle, which act to restrict mass transport into and out of the occluded site (Szklarska-Smailowska, 1986; Burstein and Mattin, 1996; Frankel, 1998). As such, repassivation can occur if the second phase particle dissolves or falls out, or if the pit covering dissolves, leading to a dilution of the pit electrolyte by the bulk environment. Increases in the chloride concentration can aid in the development of these pit coverings by making it easier to achieve saturation for metal chloride complexes resulting in precipitation and increased resistance to repassivation.

Changes in temperature are generally accepted as having an influence on nucleation and stabilization of localized corrosion, with increases in temperature aiding in these processes. Such has been observed with regard to E_{pit}, though little data exist for iron and carbon steels (Szklarska-Smailowska, 1986). In the present study, both E_{pit} and E_{rp} were observed to decrease with increasing temperature. The dependence of E_{pit} on temperature, however, was also a function of chloride concentration, as illustrated in figure 4-1 for pH 9.5 solutions. As can be seen, at high chloride concentrations, E_{pit} follows the expected inverse dependence on temperature, although the dependence is weak. At low chloride concentrations, a direct dependence of E_{pit} on temperature is observed. Lian and Jones (1998) similarly observed an increase in E_{pit} with increasing temperature for 1016 carbon steel in 10X, 100X and 1,000X J-13 water. These authors attributed the improvement in pitting resistance with increasing temperature to the formation of protective silicate films at higher temperatures. In the present case, though, no silicates were present that could lead to the formation of protective silicate films, and thus this mechanism explaining a direct dependence of E_{pit} on temperature is not valid. The weak dependence of the critical potentials on temperature may be because of an increase in passivation kinetics at higher temperatures. Thus, at low chloride concentrations, increasing the temperature aided in passivation and resulted in increasing E_{pit}. The exact mechanism and the variability in

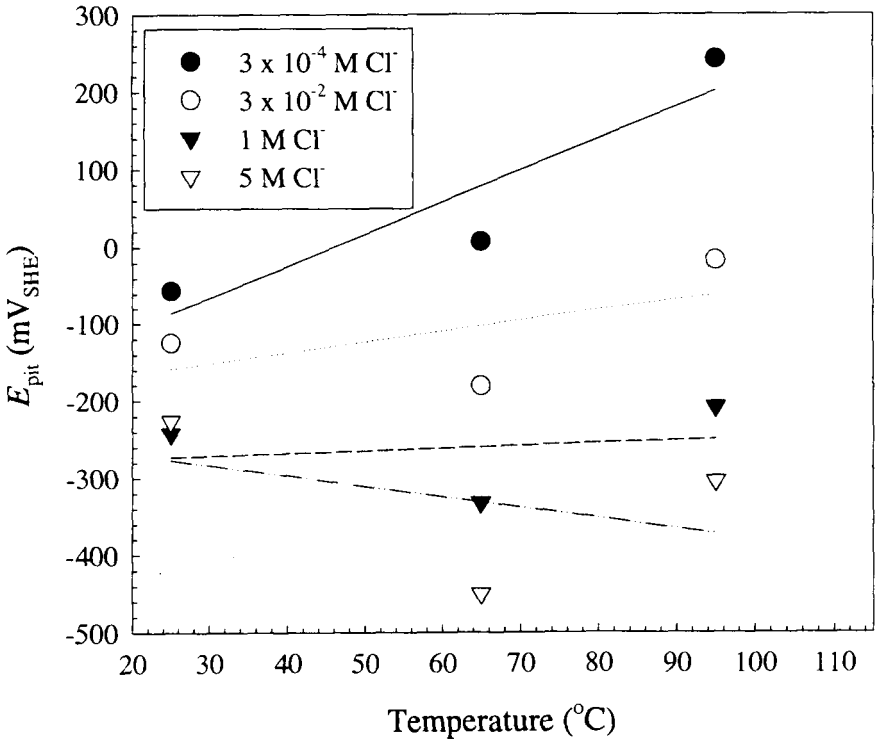

Figure 4-1. Effect of temperature on E_{pit} for A516 in deaerated 0.012 M HCO_3^-/CO_3^{2-} solution at pH 9.5 and varied chloride concentration

the dependence of E_{pit} on temperature are not clearly understood, however, and further work examining the role of temperature on the localized corrosion behavior of A516 steel is needed.

4.1.2 Potentiostatic Pitting and Crevice Tests

To further evaluate the effects of carbonate and chloride concentration, and temperature on the localized corrosion behavior of A516 steel, a series of potentiostatic pitting and crevice tests were performed. In these tests, the carbonate/chloride concentration ratio and temperature were varied and the extent of attack was evaluated via a visual rating and weight loss measurements. No clear dependence of the extent of attack during pitting corrosion on the solution composition or temperature was observed. Rather, experiments conducted under nearly identical conditions yielded dramatically different results ranging from moderate pitting to minor pitting to no measurable corrosion (minor general corrosion). Further, when considering only general corrosion or pitting corrosion as separate sets of results, no clear dependence on solution composition or temperature was observed. For example, at 20 °C severe pitting was observed at carbonate:chloride ratios of 30 and 0.425, whereas at a ratio of 21.3, only moderate pitting was observed. Heretofore, most applications of extreme value statistical analysis to pitting corrosion have been concerned with the depth of pit propagation (Marsh and Taylor, 1988) with the assumption that pit initiation times would be relatively short and thus not important in assessing WP performance. The results of the pitting tests and the lack of a discernable pattern is indicative of the stochastic nature of pit initiation (Shibata and Takeyama, 1977; Szklarska-Smailowska, 1986) and, thus, further work examining the application of statistical analysis to pit initiation times is warranted.

In an attempt to increase the consistency of the results, crevice testing as a function of solution composition and temperature was also performed. As was shown in figure 3-7, there was a clear dependence of the extent of attack and weight loss measured on the carbonate:chloride ratio (lower ratio—higher chloride concentration—more severe attack) and on temperature (higher temperature—more severe attack). These results are consistent with the extensive body of literature on the effects of chloride concentration and temperature on localized corrosion (Szklarska-Smialowska,1986). Further, it is clear that the presence of the crevice former aided in the initiation of localized attack, as would be expected (Szklarska-Smailowska, 1986). This arises because of the restriction in mass transport into and out of the occluded site by the crevice former, as development of a critical solution chemistry has been generally accepted as being a critical factor in initiating localized corrosion (Szklarska-Smailowska, 1986). Further work is planned aimed at refining the solution composition boundaries between the different regions denoting the extent of attack required, which would aid in bounding the environments where extensive localized corrosion of A516 occurs and those environments that are moderately benign from a localized corrosion standpoint.

4.1.3 Experiments on Pit Stability and Growth

Pitting corrosion that leads to perforation of the carbon steel outer overpack has received considerable attention (Cragnolino et al., 1998; Marsh and Taylor, 1988; Beavers et al., 1990). Marsh and Taylor (1988) observed pits approaching a maximum depth of 3.5 mm on carbon steel after polarization in 1,000 ppm chloride solution of pH 8.4 at 90 °C for 10,000 hr. Applying extreme probability statistical analysis to their data, they predicted that a penetration depth of 200 mm could be reached in 1,000 yr via Eq. (4-1)

$$P = 8.35\,t^{0.46} \tag{4-1}$$

where P is the maximum penetration depth in mm and t is time in years. Beavers et al. (1990), using a simulated pit electrode in which a pit specimen surrounded by a boldly exposed specimen that was tested in both the coupled and uncoupled conditions, examined pit propagation rates as a function of pit aspect ratio (pit diameter to depth). When the pit walls were insulated and the aspect ratio was 1:5, a pit propagation rate of approximately 470 μm/yr was observed. When the pit walls were allowed to freely corrode in the system, however, the pit propagation rate decreased by nearly two orders of magnitude. Thus, with pit walls insulated, a 10 cm section of carbon steel would experience perforation in roughly 200 yr, on the order of the times predicted by the expression derived by Marsh and Taylor (1988). When the pit walls were allowed to freely corrode (as would be expected to occur), the time to perforation for a 10 cm section of carbon steel increases to greater than 20,000 yr. Given that pit walls would be expected to be active during the pitting process, and thus widen out the pit mouth, and because of potential IR drop effects within deep pits (Marsh and Taylor, 1988), it is uncertain if pit stability and continued propagation could occur that would lead to perforation of 10 cm thick sections. Thus, further examination of pit stabilization mechanisms on iron and carbon steel is needed.

One of the proposed mechanisms for the stabilization of pits in chloride solutions is through the precipitation of a metal-chloride salt film (Beck, 1990; Boehni and Hunkeler, 1990; Sridhar and Dunn, 1997; Beck and Alkire, 1979; Vermilyea, 1971). Under these conditions, the dissolution rate of the metal exceeds the rate of transport of metal-chloride complexes out of the occluded site such that the pit solution becomes supersaturated with respect to metal chloride. The metal chloride salt then precipitates on the metal surface forming a salt film. This precipitated salt film controls the dissolution rate of the underlying metal (and thus the pit propagation rate) via the rate of diffusion of species through the film. Investigations of localized corrosion repassivation (Gaudet et al., 1986: Sridhar and Dunn, 1997) have shown that while the formation of a salt film does indeed stabilize pit growth, repassivation did not occur as a result on salt film dissolution. Repassivation of pits in stainless steel and Alloy 600 (Gaudet et al., 1986) occurred only after the chloride concentration within the pits decreased to below 17 percent of saturation. Similar results were observed by Sridhar and Dunn (1997) for simulated pits (figure 2-1b) of high purity nickel. For iron and carbon steels, however, the minimum chloride concentration necessary for pit initiation in iron is less than 3×10^{-3} M (Szklarska-Smialowska, 1986). As a result, pit stabilization in solutions containing higher chloride concentrations may be dependent on the pH within the actively corroding cells (Szklarska-Smialowska, 1986). As the metal corrodes, the hydrolysis of metal cations consumed OH^- and decreases the solution pH. The formation of locally acidic regions can dissolve the passive films on iron and lead to cells of active dissolution. Stabilization of the actively growing pits occurs as a result of the highly localized acidic environment that both accelerates the iron dissolution rate and prevents formation of a passive film within the pit.

In the present study, a pure iron wire was placed in a glass sheath to form a simulated 1D pit. The dimensions of the apparatus were such that the diameter of the pit was 2 mm and the depth was 10 mm, giving an aspect ratio (diameter to depth) of 1:5. After polarization of this electrode in an acidified chloride solution for a time, a precipitate was observed to form on the metal surface and over long-term exposure was nearly 1 mm thick and appeared gel-like in nature. Characterization of the precipitate using *in situ* Raman spectroscopy revealed that the film was primarily composed of $FeCl_2$, as evidenced by the close agreement between the peaks at 150, 177, 208, and 308 cm^{-1} on both the spectra of the salt film and the spectra of $FeCl_2 \cdot 4H_2O$. These results are in line with what was observed by Isaacs (1973) who similarly observed the precipitation of a gel-like film on iron in chloride solutions and proposed that the film was predominantly ferrous chloride. The peak at 490 cm^{-1} is most likely because of the glass sheath and the glass wall of the cell. The small peaks at 709 and 1,413 cm^{-1}, however, may be the result of γ-Fe_2O_3, which exhibits strong Raman peaks at 717 and 1,412 cm^{-1}. After stabilization of the salt film at +1.142 V_{SHE}, the potential was

systematically decreased in 0.45 V increments and the current response monitored. Each decrease in potential resulted in an instantaneous decrease in the current, which then rapidly increased back to its value prior to the potential step. Similar results were observed by Sridhar and Dunn (1997) examining salt film precipitation in simulated pits on nickel. This was observed to hold down to -0.208 V_{SHE}, which is approximately 200 mV above the open circuit potential of iron in this system. All these results lend credence to the theory that salt film precipitation occurs on iron in acidified chloride solutions and that this film is responsible for determining the rate of dissolution via diffusion of species through the film.

Even though these results were obtained in acidified solutions using pure iron, there are potential implications on the performance of carbon steels in the repository environment. If stabilization of localized corrosion of carbon steel in the environments likely to be found in the repository occurs via the formation of a salt film in the pit, then the propagation rate would be dictated by the diffusion of species through the film. Further, it has been well established that when pitting propagates under diffusion control, the pits tend to be hemispherical in nature (Boehni and Hunkeler, 1990; Frankel, 1998) because the diffusion distance from the center of the pit is equidistant to all points within the pit. Based upon the results of Beavers et al. (1990) using a simulated pit in which the pit walls were active, the pit propagation rate was observed to dramatically decrease compared to the case where the pit walls were inactive. Thus, it would seem that the potential exists for extensive lateral pit growth, or pit widening. This, in combination with the IR drop associated with the salt film, could likely lead to pit arrest, as mentioned by Marsh and Taylor (1988).

Examination of meteoritic iron and iron archeological objects, however, revealed extensive propagation of localized corrosion even when the environment to which the specimens are exposed is relatively dry. Corrosion of iron meteorites has been ascribed to the presence of akaganeite (β-FeOOH) in contact with the metal (Buchwald and Clarke, 1989) and not because of the presence of $FeCl_2$ salt films within pits. Akaganeite has been found to contain a considerable concentration of chloride within its lattice (up to 13 percent), and thus, continued localized corrosion penetration was possible under these circumstances, because of the continued presence of chloride from the akaganeite. In examination of unearthed archeological objects, Turgoose (1985; 1989), though, proposed that continued corrosion proceeded due to the presence of $FeCl_2$, and that akaganeite formed from oxidation of the iron chloride already present within the pit. Even though some uncertainty exists concerning the exact mechanism by which continued pit growth takes place in meteoric and archeological iron and if an iron chloride salt film is required, the observation that this does take place and continues over time frames of interest in the repository program (centuries to hundreds of thousands of years) and makes continued investigation in this area necessary.

4.2 NICKEL-BASE ALLOYS

4.2.1 Effect of Environment on Localized Corrosion Susceptibility

The combined results of CPP and long-term tests have shown that the E_{rp} is a threshold parameter for the initiation of localized corrosion. A complete discussion of the validity of using the E_{rp} as a parameter to predict the onset of localized corrosion has previously been presented (Dunn et al., 1997). Data presented for Alloy 825 clearly indicated that the E_{rp} is independent of solution pH over the range of 1 to 8. While only a limited number of E_{rp} measurements have been performed on Alloys 625 and C-22, these higher alloys are expected to exhibit E_{rp} values similarly independent of pH.

The results presented previously by Gruss et al. (1998) and discussed here suggest that the main improvement in performance gained from using Alloy 625 instead of Alloy 825 would occur at chloride concentrations less than 0.1 M. At higher chloride concentrations, the values of E_{rp} for Alloys 625 and 825 are quite similar. This observation is consistent with comparisons of performance of type 316L SS and Alloy 825 (Dunn et al., 1997). In solutions containing less than 10^{-3} M chloride, the E_{rp} values for both type 316L SS and Alloy 825 were high and localized corrosion was not initiated consistently. The E_{rp} for type 316L SS decreased at chloride concentrations around 1×10^{-3} M and the initiation of localized corrosion was consistently observed in CPP tests. Higher chloride concentrations (0.010 M) resulted in substantial decreases in the E_{rp} of Alloy 825.

The E_{corr} measurements presented in figures 3-10 and 3-15 indicate that Alloy 825 is susceptible to localized corrosion in an aerated 1,000 ppm (0.028 M) chloride solution. The initial E_{corr} measurements shown in figure 3-15 were well below the E_{rp} as a result of the poorly formed oxide film on the chromium depleted mill finished specimen surface (Dunn et al., 1995). The fluctuations of E_{corr} during the initial exposure period are likely a result of the intermittent formation and dissolution of passive films. Since the original material was deficient in chromium, the oxide film formed on the specimen surface is a poor barrier to dissolution and easily disrupted. After approximately 500 days, most of the deficient layers were removed and the passive dissolution rate decreased shifting the corrosion potential of the specimen to higher values. As the potential increased, weak spots in the passive film actively dissolved resulting in decreased values of E_{corr}. When the weak spots were removed the passive dissolution rate decreased and the E_{corr} increased. Small weak spots that were quickly removed can be expected to cause both sudden decreases, followed be rapid increases in the E_{corr}. Initiation of localized corrosion was observed only when E_{corr} was greater than E_{rp}. Reductions in the E_{corr} observed in figure 3-15 can be attributed to the active dissolution in the localized corrosion sites reducing the overall value of the E_{corr}. Repassivation of the localized corrosion sites occurred when the E_{corr} decreased below E_{rp}. The possibility of long-term evolution of the corrosion potential to values well above the E_{rp} emphasizes the need to both perform corrosion potential measurements in the environment of interest and strengthen the ability of mechanistic models to predict time dependent changes in the E_{corr} (Dunn et al., 1997).

The regression equation for E_{rp} of Alloy 825 has been used to evaluate the performance of containers (Mohanty et al., 1997). Corrosion potential calculations based on the kinetics of the anodic dissolution and cathodic reduction reactions were compared to the E_{rp} obtained with the regression equation at the chloride concentration estimated for the near-field environment. Conditions where the localized corrosion of Alloy 825 could be initiated are limited to conditions where E_{corr} is greater than E_{rp}. The approach used in EBSPAC is not limited to Alloy 825. The kinetics of oxygen reduction reactions as well as the passive anodic dissolution rates can be expected to be similar for all the candidate corrosion resistant Ni-Cr-Mo alloys. Provided that the functional dependence of E_{rp} is well defined and the E_{corr} of the candidate materials can be calculated, the criteria used to predict the onset of localized corrosion as a function of environmental conditions expected in the repository combined with a pit propagation rate can serve as a basis for predicting the long-term performance of the WP.

The initiation and repassivation potentials for the three Ni-Cr-Mo alloys plotted in figure 3-13 indicated that aggressive conditions are necessary to initiate localized corrosion of Alloy C-22. Measured values of the E_{rp} for Alloy C-22 in 4 M chloride are approximately 1,000 mV greater than the E_{rp} of either Alloys 825 or 625. Alloy C-22 can be expected to perform significantly better than the other candidate corrosion resistant alloys in hostile environments. Previous evaluations of the corrosion resistance of a variety of Ni-Cr-Mo alloys have been reported by Manning et al. (1983). The critical pitting temperature (CPT) for Alloy C-22 was measured to be 120°C during a 24-hr exposure in a solution containing 7 vol %

H_2SO_4, 3 vol % HCl, 1 wt % $FeCl_3$, and 1 wt % $CuCl_2$. Other alloys such as C-276, C-4, and 625 had lower CPTs. Other results published by Manning et al. (1983) show that the uniform corrosion rate of Alloy C-22 in a variety of acid solutions is lower than Alloy C-276. Significant uniform corrosion rates (>0.3 mm/yr) were only observed in extremely aggressive solutions such as boiling HCl, boiling HNO_3, boiling H_2SO_4 + HCl, and HF solutions. The CPT and general corrosion rate measurements, however, are only useful in ranking the relative performance of the alloys tested. The CPT can be taken as the temperature where the E_{rp} of the alloy is suppressed far enough below the E_{corr} such that pitting is initiated in a 24-hr exposure. The CPT measurement is not conservative since crevice corrosion can typically be initiated during shorter exposure times and lower temperatures (Renner et al., 1986). The results presented in figure 3-14 suggest that long times, on the order of several hundred days, are necessary to obtain conservative initiation potential measurements for a constant set of exposure conditions. CCT measurements (Renner et al., 1986) in a highly oxidizing chloride solution (10 wt % $FeCl_3$) confirm that Alloy C-22 is more resistant to localized corrosion than Alloy 625. Renner et al. (1986) reported that no pitting or crevice corrosion of Alloy C-22 was observed in 10 wt % $FeCl_3$ at temperatures up to 80 °C. Alloy 625 was found to have a CPT of 80 °C and a CCT of 60 °C in the 10 wt % $FeCl_3$ solution. During extended exposure tests, however, both the CPT and CCT were observed to decrease with time.

Rebak and Koon (1998) performed CPP tests of Alloy C-22 in 0.1 to 10 percent NaCl at 90 °C to measure E_{pit} and E_{rp}. Their results were similar to the test data shown in figure 3-12. During the forward or anodic portion of the scan, a well defined passive dissolution region was observed followed by a rapid increase in current density at potentials above 500 mV_{SHE}. The scanning direction was reversed at a current density of 10^{-3} A/cm^2. During the reverse scan, high current densities at least one order of magnitude above the passive current density of 5×10^{-7} A/cm^2 were measured until the potential was reduced below 340 mV_{SHE}. Although the hysteresis in the polarization scan suggested pitting corrosion had occurred, post-test examination of the specimen with a scanning electron microscope did not reveal any regions localized attack. The results obtained by Rebak and Koon (1998), as well as studies performed at the CNWRA (Sridhar et al., 1995), emphasize the need to perform post-test inspections of the specimens to verify that the initiation and repassivation of pitting corrosion has taken place rather than assuming that a hysteresis in the CPP scan is a positive indication of localized corrosion. In the case of Alloy C-22, other reactions, such as the evolution of oxygen or the transpassive dissolution of chromium may be responsible for the existence of a hysteresis loop in the CPP curves.

Long-term exposures of several candidate corrosion resistant alloys in solutions containing up to 28,000 ppm chloride (0.78 M) at 90 °C have been reported by Wang et al. (1998). All test specimens were electrically isolated from one another. Exposure of numerous Alloy C-22 specimen types, including welded, U-bend, and creviced, for periods of several months resulted in no initiation of localized corrosion. Small pits were observed, however, under a crevice forming device in contact with an Alloy 825 specimen. Unfortunately, the corrosion potential of the test specimens was not measured during the exposure test. Although no effort was made to deaerate the solution, the dissolved oxygen concentration in the test solution is not known. The fact that localized corrosion was observed on Alloy 825 and not on Alloy C-22 suggests the corrosion potential of the Ni-Cr-Mo alloys is greater than E_{rp} of Alloy 825 but less than E_{rp} of Alloy C-22.

Stress corrosion cracking (SCC) of Alloys C-22, G-30, C-4, 625, and titanium grade 12 in a 5 wt % NaCl solution adjusted to pH 2.7 and a temperature of 90°C was reported by Roy et al. (1998). These tests were performed with fatigue precracked double cantilever beam (DCB) specimens exposed to an environment deaerated with N_2 under open circuit conditions. Although the E_{corr} of the specimens was not measured, the solutions did not contain strong oxidants that would be capable of raising the E_{corr} above the E_{rp} for Alloy C-22. Previous investigations of Alloy 825 and type 316L SS have systematically shown that

the initiation and propagation of SCC did not occur unless the potential of the specimen was maintained above the E_{rp} (Sridhar et al., 1995). Investigations of the localized corrosion susceptibility of Alloy C-22 preformed by Gruss et al. (1998) found that crevice corrosion only occurred in 4 M chloride adjusted to pH 2.5 when the potential of the specimen was 825 mV_{SHE}. No localized corrosion was observed in numerous CPP tests performed in solutions containing less than 4 M chloride. For the tests performed by Roy et al. (1998), initiation of SCC is not considered since a sharp precrack already exists in the specimen on exposure to the solution. The E_{corr} of the Alloy C-22 specimens in the test solution used by Roy et al. (1998) can be expected to be several hundred millivolts below the E_{rp}. In addition the results of Rebak and Koon (1998) suggest that Alloy C-22 is completely resistant to localized attack in 5 percent NaCl at 90 °C, even at potentials above the E_{rp} measured in CPP tests. The reported occurrence of SCC in such relatively mild environment should be independently investigated because of its importance in assessing the performance of Alloy C-22 as a container material.

4.2.2 Galvanic Coupling Effects

The effect of the environment on the galvanic coupling of the Corrosion Allowance Material (CAM) and Corrosion Resistant Material (CRM) barriers was also examined. The effect of solution pH on the E_{corr} of Alloy 825 and A516 steel specimens in direct contact with each other was shown to be significant (figure 3-16). Large fluctuations in the E_{corr} were observed in chloride containing solution when the pH was greater than 8. Pitting of the A516 steel specimen was also observed after testing in solutions of pH 8 and above. In addition to the repeated pit initiation and repassivation events that cause the large fluctuations in the E_{corr}, there is a clear trend toward higher average values of E_{corr}. The average value of E_{corr} for the Alloy 825–A516 steel couple tested in a 1,000 ppm chloride solution at pH 10.8 increased from -300 to -200 mV_{SHE} over 8 days. Longer test periods would be required to determine the maximum potential attained by the galvanic couple under these conditions.

The value of E_{corr} without galvanic coupling and under various coupling conditions is shown in figures 3-17 to 3-19. Polished and passivated Alloy 825 specimens that were uncoupled (figure 3-17) or inefficiently coupled through a nonconductive oxide, oxyhydroxide, or corrosion product had E_{corr} values in the range of 100–300 mV_{SHE}. The high values of E_{corr} in these alloys is near the E_{rp} for Alloy 825 in a 1,000 ppm chloride solution (typically 300–400 mV_{SHE}). Evolution of the E_{corr} to higher values may occur as the passive film on the Alloy 825 surface ages and the passive current density decreases.

Large variations in the E_{corr} were observed for Alloy 825 and A516 steel specimens coupled through a layer of Fe_3O_4. These results are somewhat surprising since the high electronic conductivity of Fe_3O_4 would be expected to provide efficient galvanic coupling between the materials (Wilhelm, 1988). High values of E_{corr} seen during the initial stages of exposure (figure 3-18) may be a result of the reduction of Fe_3O_4, which occurs at potentials significantly higher than the thermodynamically calculated values (Hickling, 1973). If this were the mechanism responsible for the increased E_{corr} of Alloy 825, it follows that the E_{corr} of A516 steel should also be elevated. From figure 3-18 it is apparent that the E_{corr} of A516 increases only after the efficiency of the galvanic coupling increases and the E_{corr} of Alloy 825 drops to values in the range of -400 mV_{SHE}. Therefore, the initially high E_{corr} of Alloy 825 can be attributed to the initially inefficient coupling to A516 steel. These results are contrary to those predicted with model calculations assuming highly efficient galvanic coupling between Alloy 825 and A516 steel as a result of the high electronic conductivity of Fe_3O_4 (Wilhelm, 1988).

Data shown in figure 3-19 indicate that both $FeCl_3$ and β-FeOOH can increase the E_{corr} of Alloy 825 enough to initiate localized corrosion. The numerous small pits on the Alloy 825 specimen coupled to A516 steel through a layer of $FeCl_3$ indicate the Alloy 825 surface was not efficiently galvanically protected from localized corrosion. Some areas of attack were also found on Alloy 825 coupled to A516 steel through β-FeOOH. Results obtained with $FeCl_3$ are not surprising in view of the well known redox behavior of this compound. Substantial increases in the E_{corr} of Alloy 825 in contact with β-FeOOH should be more rigorously examined since layers of β-FeOOH have been identified as a corrosion product on A516 steel when a salt layer consistent with the dissolved species in YM groundwater is deposited on specimens subsequently exposed to humid air (Gdowski, 1998).

5 SUMMARY AND CONCLUSIONS

The purpose of this work was to further characterize the effects of experimental conditions (i.e., solution chemistry, potential, temperature) on the localized corrosion behavior of A516 steel and several Ni-base alloys in support of the NRC HLW Program. In so doing, greater insight is gained into the processes that could lead to premature failure of WPs in the repository near-field environment. Further, the main objective of the laboratory investigations of the effects of the environment on container performance is to provide sound, scientific input into EBSPAC to improve the ability of the code to accurately predict the onset and propagation rate of corrosion.

The corrosion behavior of A516 carbon steel has been shown to be a complex function of environmental conditions. The critical potentials (E_{pit} and E_{rp}) were both observed to be logarithmically dependent on the chloride concentration present in the environment. Some dependence on pH was also observed, however it seems likely that the improved resistance observed in the present study upon increasing the pH was because of competitive adsorption of carbonate with chloride (carbonate concentrations increased with increasing pH). The critical potentials were found to be weakly dependent on temperature and this dependence was a function of the chloride concentration of the solution. When potentiostatic pitting tests were conducted at potentials above the E_{rp} found from CPP tests as a function of environmental conditions (i.e., chloride and carbonate concentration, temperature), no systematic relationship was observed between the extent of attack or the type of attack (both pitting and general corrosion were observed). When similar tests were performed examining crevice corrosion, a more clear dependence of the extent of attack on chloride and carbonate concentrations and temperature emerged. The extent of attack increased with increasing temperature and with decreasing carbonate:chloride concentration ratio. Examination of a simulated pit on iron revealed that iron-chloride salt film precipitation can occur and this salt film can control the rate of metal dissolution via diffusion of species through the film.

Similar to the work done on A516 steel, E_{pit} and E_{rp} for Alloys 625, 825, and C-22 were determined as a function of environmental conditions. Alloy 625 was found to be more resistant to localized corrosion than Alloy 825 at low chloride concentrations (< 0.1 M). At high chloride concentrations, however, the differences in resistance to localized corrosion for Alloys 625 and 825 were insignificant. Alloy C-22, on the other hand, was observed to be virtually impervious to pitting at chloride concentrations up to 4 M. Long-term tests on Alloy 825 revealed that localized corrosion may initiate in air-saturated solutions at 95 °C with as little as 1,000 ppm (0.028 M) chloride. Galvanic coupling of the Ni-base inner barrier to the A516 steel outer barrier could extend the life of the WPs with Alloy 825 or 625 inner barriers, only if highly efficient galvanic coupling is maintained.

6 FUTURE WORK

6.1 CARBON STEEL

To further investigate whether a 10 cm thick sections of carbon steel can be perforated via pitting in the repository environment, three sets of experiments are planned. First, long-term (5+ yr) tests are planned to continue the potentiostatic tests to longer timeframes. In these tests, the effects of surface finish (mill scale versus polished), crevice formation, temperature, aeration (aerated versus deaerated) and solution composition on localized corrosion, and in particular, penetration rates, will be examined. The results of these tests will expand our understanding of the role and interactions of surface finish and environment and provide experimental data as to the propensity for carbon steel to experience sustained pit propagation to large depths. It is anticipated that a series of samples will be exposed simultaneously and then certain samples will be removed periodically from testing and evaluated for extent of attack. This will also afford an opportunity to further examine the potentially statistical nature of pit initiation, which may have a significant effect on WP lifetime predictions.

The second and third sets of experiments are designed to investigate the role of salt film precipitation on pit stability. This process has been proposed as an operative mechanism and the salt film is recognized as playing a controlling factor in the dissolution rate inside the pit. Furthermore, it has been suggested in the literature that dissolution of a precipitated salt film is critical to pit arrest and repassivation. The results from the planned experiments in this area will attempt to address this possibility on iron. Work will also begin using simulated pit electrodes similar to that used by Beavers et al. (1990) in which the pit walls are allowed to freely corrode as well as a new segmented electrode design that should enable lateral propagation rates to be examined as a function of pit depth (aspect ratio) and environment.

Another area of potential investigation is the impact that potential fabrication methods may have on the corrosion resistance of carbon steels. Welded sections of carbon steel suffer from "grooving corrosion," selective attack on the weld, when exposed to seawater (Szklarska-Smialowska, 1986). Welding has also been shown to result in impurity segregation at weldments, which could also be detrimental to corrosion resistance as well as thermal stability (Szklarska-Smialowska, 1986; Cragnolino et al., 1998). Furthermore, as a stress relief heat treatment is anticipated after welding, the degree of stress relief could be a critical factor in determining the susceptibility of A516 steel to SCC originating at the welds. Given the temperatures necessary for near complete stress relief (~650 °C), it may be necessary to only perform partial stress relief heat treatments and thus some residual stresses may still be present (Krauss, 1990; Cragnolino et al., 1998). Thus, examination of the potential detrimental effects of fabrication methods on the corrosion behavior of A516 steel will need further investigation once the container materials and fabrication methods are finalized.

6.2 NI-BASE ALLOYS

Even though considerable effort has been spent examining the corrosion behavior of Ni-base alloys, a number of issues remain that should be evaluated, particularly with respect to Alloy C-22. These issues include the range of potential and environmental conditions for susceptibility to SCC, evaluation and measurement of the corrosion behavior of Alloy C-22 above 100 °C (specifically, the passive current density, and the pitting and repassivation potentials) to predict the behavior below the boiling point, and issues related to fabrication methods and their impact on corrosion performance.

SCC of Alloy C-22 has been recently reported to occur in acidified brine solutions at elevated temperatures (Roy et al., 1998). Using wedge loaded DCB specimens in deaerated, pH 2.7, 5 wt % NaCl at 80 °C, these authors observed no crack growth during the first month of exposure. Continued exposure, however, led to crack extensions of 0.036 in. and 0.065 in. after 5 mo exposure. Previous works, however, have found that Alloy C-22 is highly resistant to SCC until very high temperatures are reached. For example, in the review by Sridhar and Cragnolino (1992), the minimum temperature for SCC in 20.4 wt % $MgCl_2$ was reported to be over 225 °C for Alloy C-276, which is similar to Alloy C-22. Further, they reported that no Alloy C-22 SCC failures were observed during 12 mo exposure to 43 wt % $CaBr_2$ at 204 °C. Based on work examining the SCC behavior of Alloy 825, it has been demonstrated that the E_{rp} is an enabling parameter for SCC, which did not occur when the potential of the metal was below E_{rp} (Sridhar et al., 1995; Cragnolino et al., 1996). Based on this work, the E_{rp} for Alloy C22 is considerably greater than that for Alloy 825 (typically 250–800 mV at 95 °C depending on the chloride concentration). Thus, the recent claims pertaining to SCC failures on Alloy C-22 at relatively low temperatures warrant further testing and evaluation.

Because the tests conducted to date on Alloy C-22 at temperatures of 95 °C have not shown clear evidence of pitting despite the appearance of a hysteresis loop during CPP tests, it is necessary to examine the electrochemical behavior of Alloy C-22 at temperatures above 100 °C to define the critical potentials and their dependence on environmental conditions (e.g., chloride concentration, pH). Additionally, the passive current density would be measured during these tests. These results will allow a basis for comparison to previous studies on Alloys 625 and 825 and will serve as input to various computer modeling programs to predict WP lifetimes and failure modes. The results will also aid in evaluating the likelihood of SCC failures at potentials above and below E_{rp}, as highlighted previously.

The effects of fabrication methods on corrosion and possible failure modes of Alloy C-22 also should be evaluated. It was recently reported that weld spatter from carbon steel welds that collected on a type 316 L SS shaft led to SCC failure of the shaft. It was proposed that the introduction of localized stress from heating because of the weld globules and dilution of the type 316L SS base metal chemistry as a result of fusion with the weld globules and formation of corrosion products initiated the SCC (Agrawal, 1998). Weldments on stainless steels have also been found to be more susceptible to pitting corrosion, primarily because of segregation of Cr and Mo so that the inner dendritic regions in the weldment were depleted and underwent selective dissolution (Szklarska-Smialowska, 1986). Rebak and Koon (1998) similarly observed more extensive pitting attack at weldments on Alloy C-4 and C-22 after 24 hr exposure in boiling (105 °C) 23 wt % sulfuric acid + 1.2 wt % hydrochloric acid + 1 wt % copper chloride. Based on these results, further examination of the effects of fabrication methods on Alloy C-22 failure modes should be considered.

6.3 ENVIRONMENTAL EFFECTS ON ALTERNATE WASTE PACKAGE DESIGNS

Recently, design changes that would alter the WP from an Alloy C-22 inner/A516 steel outer system to an Alloy C-22 inner/Ti-alloy outer system have been proposed, primarily to significantly improve the corrosion resistance of the WP. Literature examining the corrosion behavior of Ti-alloys clearly shows these materials are highly resistant to corrosion. By altering the WP design from a thin CRM surrounded by a thick CAM to a thin CRM—thin CRM design introduces several issues that would need to be addressed: the potential for mechanical damage from handling, rock impact because of the thinner cross section, or both; radiolysis effects, as the overall wall thickness would decrease significantly to likely allow the formation of radiolysis products; and possible detrimental galvanic interactions between Alloy C-22 and Ti-alloys leading

to accelerated corrosion, SCC, or hydrogen embrittlement. The issues surrounding the importance of ensuring adequate mechanical integrity to withstand handling and rock impacts are easily understood and can likely be modeled using available information. The impact of radiolysis products on corrosion is also thoroughly recognized, although the impact of radiolysis on the corrosion behavior of Ti-alloys has not been fully evaluated. Though it may be unlikely that galvanic coupling of Alloy C-22 and Ti-alloys will lead to significant acceleration of corrosion under the conditions present in the repository, verification would be necessary.

6.4 CORROSION UNDER DRIP CONDITIONS

Other activities currently planned include examination of the time dependent chemistry variations as a result of WP emplacement in a partially saturated drift, characterization of the effect of water dripping on a heated WP surface on the near-field chemistry, and assessment of container performance under heat transfer conditions with condensed water dripping on the WP surface. This work will involve the development of suitable electrode configurations that can withstand and effectively operate during elevated temperature exposures to monitor changes in water chemistry during dripping. One possibility for accomplishing this is via the development of Application Specific Integrated Circuits, which recently have been applied to corrosion research issues.

Multiple stages are envisioned to examine corrosion under drip conditions. The first will involve a series of initial feasibility tests in which the solution chemistry and corrosion measurements are performed using a heated, flat specimen to serve as an opportunity to develop electrode designs, measurement techniques, and overall system geometry. After measurement techniques and electrode designs have been optimized, the geometry of the system will be altered to a scaled down version of a container placed in a drift. Three different configurations will potentially be considered as simulations of the WP in the repository. The first would involve dripping water under controlled flow conditions onto the top of an insulated specimen that would have a radius of curvature comparable to the actual WP, heated to above boiling (approximately 110 °C). This configuration would be used to simulate and examine the initial stages of WP wetting and the degradation that occurs during this time period. The second possible configuration would involve dripping and collecting water underneath an insulated specimen that would have a radius of curvature comparable to the actual WP, heated to temperatures just below boiling (approximately 95 °C). This configuration would be used to simulate and examine the later stages of WP corrosion in which the sample was already wetted and water was collecting in the crevice formed between the bottom of the WP and the pier. The third possible configuration would be to design a scaled down WP and locate it within a simulated drift. The temperature of the specimen surface will be controlled by a heater placed inside the specimen with controlled water flow originating through the simulated drift. This configuration would allow the surrounding rock and geological environment to influence WP degradation.

7 REFERENCES

Agrawal, A.K. 1998. Weld spatter unexpectedly lowers the boom. *Materials Performance* 37(2): 102–104.

Alvarez, M.G., and J.R. Galvele. 1984. The mechanism of pitting of high purity iron in NaCl solutions. *Corrosion Science* 24: 27–48.

American Society for Testing and Materials. 1996a. Standard test method for conducting cyclic potentiodynamic polarization measurements for localized corrosion susceptibility of iron-, nickel- or cobalt-based alloys. *Annual Book of Standards*. West Conshohocken, PA: American Society for Testing and Materials 03.02: 224–231.

American Society for Testing and Materials. 1996b. Standard practice for laboratory immersion corrosion testing of metals. *Annual Book of Standards*. West Conshohocken, PA: American Society for Testing and Materials: 03.02: 89–96.

Beavers, J.A., N.G. Thompson, and A.J. Markworth. 1990. Pit propagation of carbon steel in groundwater. *Advances in Localized Corrosion*. Houston, TX: NACE International: 165–174.

Beck, T.R. 1990. Occurrence and properties of anodic salt films in pitting corrosion. *Advances in Localized Corrosion*. Houston, TX: NACE International: 85–91.

Beck, T.R., and R.C. Alkire. 1979. Occurrence of salt films during initiation and growth of corrosion pits. *Journal of the Electrochemical Society* 126: 1,662–1,666.

Bird, H.E.H., B.R. Pearson, and P.A. Brook. 1988. The breakdown of passive films on iron. *Corrosion Science* 28: 81–86.

Boehni, H., and F. Hunkeler. 1990. Growth kinetics and stability of localized corrosion processes. *Advances in Localized Corrosion*. Houston, TX: NACE International: 69–75.

Buchwald, V.F., and R.S. Clarke. 1989. Corrosion of Fe-Ni alloys by Cl-containing akaganeite: The antarctic meteorite case. *American Mineralogist* 74: 656–667.

Burstein, G.T., and S.P. Mattin. 1996. The nucleation and early stages of growth of corrosion pits. *Critical Factors in Localized Corrosion II*. Pennington, NJ: The Electrochemical Society: 1–14.

Cragnolino, G.A., and N. Sridhar. 1991. Localized corrosion of a candidate container material for high-level nuclear waste disposal. *Corrosion* 47: 464–472.

Cragnolino, G.A., D.S. Dunn, and N. Sridhar. 1996. Environmental factors on the stress corrosion cracking of type 316L stainless steel and alloy 825 in chloride solutions. *Corrosion* 52: 194–203.

Cragnolino, G.A., D.S. Dunn, P. Angell, Y.-M. Pan, and N. Sridhar. 1998. Factors influencing the performance of carbon steel overpacks in the proposed high-level nuclear waste repository. Paper No. 98-147. *Corrosion/98*. Houston, TX: NACE International.

Degen, I.A., and G.A. Newman. 1993. Raman spectra of inorganic ions. *Spectrochimica Acta* 49A: 859–887.

Dunn, D.S., and G.A. Cragnolino. 1997. *An Analysis of Galvanic Coupling Effects on the Performance of High-level Nuclear Waste Container Materials*. CNWRA 97-010. San Antonio, TX: Center for Nuclear Waste Regulatory Analyses.

Dunn, D.S., and G.A. Cragnolino. 1998. *Effect of Galvanic Coupling between Overpack Materials of High-Level Nuclear Waste Containers—Experimental and Modeling Results*. CNWRA 98-004. San Antonio, TX: Center for Nuclear Waste Regulatory Analyses.

Dunn, D.S., G.A. Cragnolino, and N. Sridhar. 1997. *An Electrochemical Approach to Predicting Long-Term Localized Corrosion of Corrosion Resistant Container Materials*. San Antonio, TX: Center for Nuclear Waste Regulatory Analyses.

Dunn, D.S., G.A. Cragnolino, and N. Sridhar. 1998. Effect of galvanic coupling between overpack materials for high-level nuclear waste containers. Paper No. 98-148. *Corrosion/98*. Houston, TX: NACE International.

Dunn, D.S., N. Sridhar, and G.A. Cragnolino. 1995. Effects of surface chromium depletion on localized corrosion of alloy 825 as a high-level nuclear waste container material. *Corrosion* 51(8): 618–624.

Dunn, D.S., N. Sridhar, and G. Cragnolino. 1996. Long-term localized corrosion of alloy 825 in high-level nuclear waste repository environments. *Corrosion* 52: 115–124.

Frankel, G.S. 1998. Pitting corrosion of metals, a review of the critical factors. *Journal of the Electrochemical Society* 145: 2,186–2,198.

Gaudet, G.T., W.T. Mo, T.A. Hatton, J.W. Tester, J. Tilly, H.S. Isaacs, and R.C. Newman. 1986. Mass transfer and electrochemical kinetic interactions in localized pitting corrosion. *AIChE Journal* 32: 949–957.

Gdowski, G. 1998. Humid air corrosion of YMP waste package material. Paper No. 151. *Corrosion/98*. Houston, TX: NACE International.

Gruss, K.A., G.A. Cragnolino, D.S. Dunn, and N. Sridhar. 1998. Repassivation potential for localized corrosion of Alloys 625 and C-22 in simulated repository environments. Paper No. 98-149. *Corrosion/98*. Houston, TX: NACE International.

Hibner, E.L. 1986. Evaluation of test procedures for critical crevice temperature determination for nickel alloys in a ferric chloride environment. Paper No. 86-181. *Corrosion/86*. Houston, TX: NACE International.

Hickling, A. 1973. The cathodic reduction potential of Fe_3O_4 and the Flade potential of iron. *Electrochemica Acta* 18: 635–637.

Isaacs, H.S. 1973. The behavior of resistive layers in the localized corrosion of stainless steel. *Journal of the Electrochemical Society* 120: 1,456–1,462.

Johnson, A.B., and B. Francis. 1980. *Durability of Metals from Archeological Objects, Metal Meteorites, and Native Metals.* PNL–3198. Richland, WA: Pacific Northwest National Laboratory.

Klein, H.J., B.H. Rosof, C.L. Jeanfils, and J.H. Chen. 1981. The argon oxygen decarburization and electroslag remelting processes. *Metallurgical Treatises.* J.K. Tien and J.F. Elliott, eds. Pittsburgh, PA: The Metallurgical Society of American Institute of Mining, Mechanical and Metallurgical Engineering: 230–259.

Krauss, G. 1990. *Steels: Heat Treatment and Processing Principles.* Materials Park, OH: ASM International.

Lian, T., and D.A. Jones. 1998. Electrochemical corrosion behavior of low carbon steel in simulated Yucca Mountain vadose waters. Paper No. 98-163. *Corrosion/98.* Houston, TX: NACE International.

Manning, P.E., and J.D. Schöbel. 1986. Hastelloy® alloy C-22—a new and versatile material for the chemical process industries. *Werkstoffe und Korrosion* 37: 137–145.

Manning, P.E., N. Sridhar, and A.I. Asphahani. 1983. New developmental Ni-Cr-Mo alloys. Paper No. 21. *Corrosion/83.* Houston, TX: NACE International, Inc.

Mao, X., X. Liu, and R.W. Revie. 1994. Pitting corrosion of pipeline steel in dilute bicarbonate solution with chloride ion. *Corrosion* 50: 651–657.

Marsh, G.P., and K.J. Taylor. 1988. An assessment of carbon steel containers for radioactive waste disposal. *Corrosion Science* 28: 289–320.

Mohanty, S., G.A. Cragnolino, T. Ahn, D.S. Dunn, P.C. Lichtner, R.D. Manteufel, and N. Sridhar. 1997. *Engineered Barrier System Performance Assessment Code: Ebspac Version 1.1.* CNWRA 97-006. San Antonio, TX: Center for Nuclear Waste Regulatory Analyses.

Mohanty, S., and T.J. McCartin. 1998. *Total-System Performance Assessment (TPA) Version 3.1.4 Code: Module Descriptions and User's Guide.* San Antonio, TX: Center for Nuclear Waste Regulatory Analyses.

Nakayama, G., H. Wakamatsu, and M. Akashi. 1993. Effects of chloride, bromide, and thiosulfate ions on the critical conditions for crevice corrosion of several stainless alloys as a material of geological disposal package for nuclear wastes. *Scientific Basis for Nuclear Waste Management XVI.* G.C. Interrante and R.T. Pabalan, eds. Pittsburgh, PA: Materials Research Society: 323–328.

Nuclear Regulatory Commission. 1998. *Issue Resolution Status Report Key Technical Issue: Container Life and Source Term.* Revision 1. G. Cragnolino, compiler. Washington, DC: Nuclear Regulatory Commission. Predecisional.

Rebak, R.B., and N.E. Koon. 1998. Localized corrosion resistance of high nickel alloys as candidate materials for nuclear waste repository: Effect of alloy and weldment aging at 427 °C for up to 40,000 hours. Paper No. 98-153. *Corrosion/98.* Houston, TX: NACE International.

Renner, M., U. Heubner, M.B. Rockel, and E. Wallis. 1986. Temperature as a pitting and crevice corrosion criterion in the $FeCl_3$ test. *Werkstoffe und Korrosion* 37: 183-190.

Roy, A.K., D.L. Flemming, and B.Y. Lum.1998. Stress corrosion cracking of Fe-Ni-Cr-Mo, Ni-Cr-Mo and Ti alloys in 90 °C acidic brine. Paper No. 98-157. *Corrosion/98*. Houston, TX: NACE International.

Sagar, B., ed. 1996. *NRC High-Level Radioactive Waste Program Annual Progress Report: Fiscal Year 1996*. NUREG/CR–6513, No.1. Washington, DC: Nuclear Regulatory Commission.

Scully, J.R. 1995. Electrochemical tests. *Corrosion Tests and Standards, Application and Interpretation*. Philadelphia, PA: American Society for Testing and Materials: 75–90.

Shibata, T., and T. Takeyama. 1977. Stochastic theory of pitting corrosion. *Corrosion* 33: 243–251.

Simard, S., H. Menard, and L. Brossard. 1998. Localized corrosion of 1024 mild steel in slightly alkaline bicarbonate solution with Cl^- ions. *Journal of Applied Electrochemistry* 28:151–160.

Sridhar, N., and G.A. Cragnolino. 1992. SCC of nickel-base alloys. *Stress-Corrosion Cracking, Materials Performance and Evaluation*. Materials Park, OH: ASM International: 131–179.

Sridhar, N., and D.S. Dunn. 1997. *In-situ* study of salt film stability in simulated pits of nickel by Raman and electrochemical impedance spectroscopies. *Journal of the Electrochemical Society* 144: 4,243–4,253.

Sridhar, N., G.A. Cragnolino, D.S. Dunn, and H.K. Manaktala. 1994. *Review of Degradation Modes of Alternate Container Designs and Materials*. CNWRA 94-010. San Antonio, TX: Center for Nuclear Waste Regulatory Analyses.

Sridhar, N., G.A. Cragnolino, and D.S. Dunn. 1995. *Experimental Investigations of Failure Processes of High-Level Radioactive Waste Container Materials*. CNWRA 95-010. San Antonio, TX: Center for Nuclear Waste Regulatory Analyses.

Strommen, D.P., and K. Nakamoto. 1984. *Laboratory Raman Spectroscopy*. New York: John Wiley and Sons.

Sussek, G., and M. Kesten. 1975. Eine Charakterisierung der lochfraβkorrosion des nickels-I die bestimmung der lochfraβ-potentiale in neutralen und alkalischen Lösunger (Ger). *Corrosion Science* 15: 225–238.

Szklarska-Smialowska, Z. 1978. Passivating anions. *Passivity of Metals*. Princeton, NJ: The Electrochemical Society: 443–462.

Szklarska-Smialowska, Z. 1986. *Pitting Corrosion of Metals*. Houston, TX: NACE International.

Tawancy, H.M., R.B. Herschenroeder, and A.I. Asphahani. 1983. High-performance Ni-Cr-Mo-W alloys. *Journal of Metals* 35: 37–43.

TRW Environmental Safety Systems. 1997. *Engineered Barrier System Performance Requirements Systems Study Report*. B00000000–01717–5705–00001. Rev. 02. Las Vegas, NV: TRW Environmental Safety Systems, Inc.

Turgoose, S. 1985. The corrosion of archeological iron during burial and treatment. *Studies in Conservatism* 30: 13–18.

Turgoose, S. 1989. Structure, composition and deterioration of unearthed iron objects. *Current Problems in the Conservation of Metal Antiquities: International symposium on the Conservation and Preservation of Cultural Property*. Tokyo, Japan: Tokyo National Research Institute of Cultural Properties: 35–53.

U.S. Department of Energy. 1998. *Repository Safety Strategy: U.S. Department of Energy's Strategy to Protect Public Health and Safety after Closure of a Yucca Mountain Repository*. YMP/96–01. Rev. 1. Washington, DC: U.S. Department of Energy, Office of Civilian Radioactive Waste Management.

Vermilyea, D.A. 1971. Concerning the critical pitting potential. *Journal of the Electrochemical Society* 118: 529–531.

Vieth, P.H., and J.F. Kiefner. 1994. *Database of Corroded Pipe Tests*. Final Report. Worthington, OH: Kiefner & Associates, Inc.

Vinson, D.W., W.M. Nutt, and D.B. Bullen. 1995. *Survey of Degradation Modes of Candidate Materials for High-Level Radioactive Waste Disposal Containers*. UCRL–CR–120464. Livermore, CA: Lawrence Livermore National Laboratory.

Wang, F., G.E. Gdowski, J. Estill, S. Gordon, S. Doughty, K. King, and D. McCright. 1998. Long-term corrosion study of the waste package candidate material for the YMP: Initial results. Paper No. 161. *Corrosion/98*. Houston, TX: NACE International.

Wilhelm, S.M. 1988. Galvanic corrosion caused by corrosion products. *Galvanic Corrosion*. H.P. Hack, ed. ASTM STP 978. Philadelphia, PA: American Society of Testing and Materials: 23–34.